Shipboard Fluid System Diagnostics using Non-Intrusive Load Monitoring

by

Gregory R. Mitchell

B.S., Naval Architecture, United States Naval Academy, 2000

Submitted to the Department of Mechanical Engineering in Partial Fulfillment of the Requirements for the Degrees of

Naval Engineer
and
Master of Science in Ocean Systems Management

at the
Massachusetts Institute of Technology

June 2007

Signature of Author _____
Department of Mechanical Engineering
May 11, 2007

Certified by _____
Steven B. Leeb
Professor of Electrical Engineering and Computer Science & Mechanical Engineering
Thesis Supervisor

Certified by _____
Robert W. Cox
Assistant Professor of Electrical and Computer Engineering, UNC Charlotte
Thesis Supervisor

Certified by _____
Henry S. Marcus
Professor of Marine Studies
Thesis Supervisor

Accepted by _____
Lallit Anand
Chairman, Department Committee on Graduate Students
Department of Mechanical Engineering

Page Intentionally Left Blank

Shipboard Fluid System Diagnostics using Non-Intrusive Load Monitoring

By

Gregory R. Mitchell

Submitted to the Department of Mechanical Engineering on May 11, 2007 in Partial Fulfillment of the Requirements for the Degrees of

Naval Engineer

and

Master of Science in Ocean Systems Management

Abstract

Systems on modern naval vessels are becoming exclusively dependent on electrical power. One example of this is the replacement of distilling and evaporator plants with reverse osmosis units. As the system is in continuous operation, it is critical to have remote real-time monitoring and diagnostic capabilities. The pressure to reduce shipboard manning only adds to the difficulties associated with monitoring such systems. One diagnostic platform that is particularly well suited for use in such an environment is the non-intrusive load monitor (NILM). The primary benefit of the NILM is that it can assess the operational status of multiple electrical loads from a single set of measurements collected at a central point in a ship's power-distribution network. This reduction in sensor count makes the NILM a low cost and highly reliable system.

System modeling, laboratory experiments, and field studies have all shown that the NILM can effectively detect and diagnose several critical faults in shipboard fluid systems. For instance, data collected from the reverse osmosis units for two U.S. Coast Guard Medium Endurance Cutters indicate that the NILM can detect micron filter clogging, membrane failures, and several motor-related problems. Field-tested diagnostic indicators have been developed using a combination of physical modeling and laboratory experiments.

Thesis Supervisor: Steven B. Leeb
Title: Professor of Electrical Engineering and Computer Science & Mechanical Engineering

Thesis Supervisor: Robert W. Cox
Title: Assistant Professor of Electrical and Computer Engineering, UNC Charlotte

Thesis Supervisor: Henry S. Marcus
Title: Professor of Marine Systems

Acknowledgements

The author would like to acknowledge the following organizations and individuals for their assistance. This thesis would not have been possible without them.

- The Office of Naval Research's Control Challenge, ONR/ESRDC Electric Ship Integration Initiative and the Grainger Foundation, all of whom provided funding
- Officers and Crew of the USCGC *Escanaba*
- Officers and Crew of the USCGC *Seneca*
- Professor Robert Cox for his enthusiasm, assistance, and feedback
- Jim Paris for his computer and NILM technical assistance
- Professor Henry S. Marcus for advisement as a thesis reader
- Professor Steven Leeb who provided me with a challenging and extremely rewarding experience
- Finally, to my wife and kids who have been exceptionally supportive throughout my graduate school experience

Table of Contents

List of Figures

List of Tables

1 Introduction

1.1 Non-Intrusive Load Monitoring

The Non-Intrusive Load Monitor (NILM) is a device that records electrical voltage and current to monitor instantaneous power demand. It is capable of monitoring single or multiple loads depending on where the sensors are mounted in relation to the electrical distribution system. The NILM's non-intrusive aspect roots from the minimal infrastructure requirements for the voltage tap and current transducer installations. Often the only physical sign of a NILM installation is an extra wire leading from a power distribution panel. The NILM operating software can be tailored to specific systems. The NILM's ability to monitor, detect, and diagnose system operating characteristics and failures by tracking only the electrical power demand contradicts recent marine industry trends [1]. These remote monitoring and automation technologies rely on vast sensor networks increasing installation and maintenance costs while adding reliability issues to an array of complex sensors.

Non-intrusive load monitoring research has been conducted at the Massachusetts Institute of Technology's Laboratory for Electromagnetic and Electronic Systems (LEES) for over two decades. The NILM has been previously utilized in residential, commercial, automotive, and marine environments [2] [3] [4]. The research presented in this thesis is from the application of NILM technology on shipboard fluid system diagnostics.

For the current shipboard NILM installation, the transient event detection and diagnostics software has yet to be fully developed. To aid in the development of the NILM diagnostics software, research is necessary to understand dynamics of shipboard systems. The research presented in this thesis is an in-depth examination and isolation of diagnostic indicators on shipboard fluid pump systems. To help understand the complex system dynamics a computer-based model was developed to simulate the system and possible diagnostic methods. A maintenance and repair cost analysis was also completed to illustrate possible advantages of utilizing the NILM for condition-based maintenance and failure detection.

1.2 Motivation for Research

The dependency on electric motive power for shipboard systems has continuously increased over the last century. This growth can be attributed to improvements in operating efficiencies and simplification of distributed systems. Electricity has proven itself as a reliable alternative to steam for energy transport throughout a ship. It also provides a complete distribution network of shipboard loads presenting the perfect platform for NILM type applications in remote system monitoring and diagnostics.

Traditionally, the monitoring has been done with watchstanders taking logs and dedicated sensors whose outputs are collected by a larger monitoring network. These sensors are often intrusive, in that they must break system integrity to monitor such characteristics as pressure or temperature. Additionally, these types of sensors require additional maintenance for calibration and reliability. Modern propulsion plant monitoring systems can have over 8,000 sensors within the main machinery space [1]. Most of the sensor available today are only capable of monitoring single system parameters and often have redundant sensors within the same system to improve the network reliability. As additional sensors are installed the wiring, complexity, weight, and cost also increases for the monitoring network. Shipboard NILM installations have the potential to avert those increases and reduce shipbuilding costs.

A majority of mechanical systems have electrical components whose operation not only depends on the component itself, but also the mechanical system to which it is attached. NILM has the ability to monitor these electro-mechanical systems with only a voltage tap and current transducer signals. Developing diagnostic indicator tools for such systems would allow NILM to provide reliable single-point monitoring at significantly less cost and complexity then conventional sensor configurations.

1.3 Thesis Objectives

The research presented in this thesis is a continuation of work conducted by LCDR Jack S. Ramsey, Jr., USN [5], LT Thomas W. DeNucci, USCG [6], and LT James P. Mosman, USN [7]. Previous research has concluded the applicability of NILM on various shipboard systems. Most recently, LT Mosman developed a diagnostic algorithm for shipboard cycling systems.

The objective of this thesis is to further explore and develop diagnostic indicators for fluid pump system maintenance and failures. Additionally, an in-depth fluid pump start transient analysis is developed to model and diagnose a filter element condition prediction method. Although the research presented is for a specific pump and filter combination, the methodologies and diagnostic indicators are applicable to many other shipboard fluid pump systems.

2 Equipment and Descriptions

2.1 NILM Overview

As shown in Figure 2-1 the NILM uses voltage and current measurements to estimate real and reactive power loads. Separate channels collect Voltage and current measurements using COTS transducers. Each voltage channel and its associated current channel are known as *pair*. The NILM records and analyzes the signals with a Pentium class PC [2] [8]. The NILM is typically configured to capture current and voltage data at a sample rate of 8,000 Hz per channel for monitoring and detecting load transients. This capture rate ensures accurate short-term transient detection and permits the NILM to analyze the spectral content created by electro-mechanical systems.

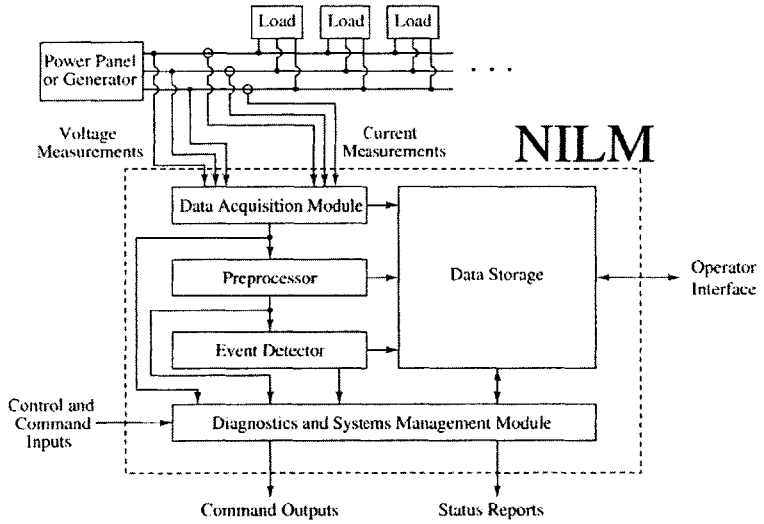

Figure 2-1: NILM Signal Path Flow Diagram [7]

The NILM is also capable of tracking the operating schedule of electrical loads on a power distribution system [9]. It uses measurements of the current flowing into the stator terminals of an induction motor to track and trend of key motor parameters and harmonics [10] [11]; thus enable a platform for condition based maintenance (CBM). Finally, the NILM's real-time monitoring makes it ideal for failure detection and diagnosis.

In a single-phase grounded system, power measurement with the NILM is relatively straightforward. The NILM is supplied with voltage from line-to-neutral and current from any

load downstream of the monitoring point. Real power is calculated using current, which is in-phase with voltage, while reactive power is calculated from current components that are 90° out of phase with voltage.

For a three-phase ungrounded electrical system, such as those on naval vessels, the power measurement is more complex. The voltage observed by the NILM is typically line-to-line (there is no ground). In addition, usually only one of the three phases is needed for the NILM to function effectively. For the three-phase system applications examined in this thesis, voltage is measured across two of the phases while the current is taken from the third.

The NILM output data can be recorded as *raw* or *prepared* (*prep*) data. On the hour, the NILM compresses the previously recorded data into a *snapshot* file with a corresponding date-time designator. The *raw* data is a two-column matrix of voltage and current at 8,000 Hz per channel pair. The *prep* data output option is formatted as an eight-column matrix that contains values for the real power, the reactive power, and their associated harmonics at only 120 Hz per channel pair. The *prep* data hourly snapshot files are 88% smaller than the corresponding *raw* data equivalent. In the case of the *prep* data, the matrix column corresponding to each of these power quantities depends on the number of electrical phases in the measured system. In a single-phase system, the values for the real power are contained in the first column of the matrix while the values for the reactive power are contained in the second column. For three-phase power these relationships are reversed; the values for reactive power are contained in the first column of the matrix while the values for the "negative" real power are contained in the first column. Table 2-1 identifies the relationships between the data collection configuration and snapshot file format.

Table 2-1: Snapshot File Format

Data Collection Type	Output Snapshot File	
	1st Column	2nd Column
Raw Data	Voltage	Current
Prep Data, Single-Phase System	Real Power	Reactive Power
Prep Data, Three-Phase System	Reactive Power	(-) Real Power

Since the A/D convert quantizes data into values that range between 0 and 4096, the current, in amps, is derived from the NILM *prep* data using Equation 2.1-1.

$$I_{NILM} = \left(\frac{D_{NILM}}{64}\right)\left(\frac{G}{4096}\right)\left(\frac{K_N}{R_{NILM}\sqrt{2}}\right) \tag{2.1-1}$$

Where: I_{NILM} = measured current from NILM (Amps)
D_{NILM} = NILM real power *prep* data
G = peak-to-peak voltage corresponding to the PCI-1710 card gain code (gain=g, 0=10, 1=5, 2=2.5, 3=1.25)
K_N = current transducer conversion ratio
R_{NILM} = NILM measuring resister size (Ohms)

Using the current calculated in Equation 2.1-1 the real power is converted to watts with Equation 2.1-2.

$$P_{NILM} = \frac{V_{NILM} \cdot I_{NILM}}{\sqrt{3}} \tag{2.1-2}$$

Where: P_{NILM} = measured real power (Watts)
V_{NILM} = measured NILM voltage (Volts)
I_{NILM} = measured current from NILM (Amps)

Although, the prep data from NILM provides a relative figure of power demand over time, by converting it to Watts the data is easily compared between multiple NILM monitored systems.

2.2 Pumps and Filters

Since most shipboard fluid systems transport liquid from one location to another they require a hydraulic forcing mechanism and a way to ensure the solution quality. These processes are typically carried out by pump-filter combinations where the NILM can monitor system through the pump motor power demand. The following sections review common pump and filter types found in shipboard fluid systems.

2.2.1 Centrifugal Pumps

Centrifugal pumps have a wide range of uses in shipboard applications. The pump works by accelerating a fluid through the centrifugal force generated by a rapidly revolving impeller [12].

The impeller action adds kinetic energy (also known as velocity head) to the fluid. The volute partially converts the fluid velocity head to static pressure head as it is discharged from the pump. In general, centrifugal pumps are considered "constant head" machines meaning that the pump speed and flow rate will vary while the discharge head remains constant [12]. This situation can occur when throttling a valve. As the valve closes, the pump flow rate decreases while the RPM increases with a constant discharge pressure. A *pump curve* describes the pump's discharge head performance as a function of the flow rate for a particular speed.

Centrifugal pumps are classified by the manner in which fluid flows through the impeller. The three basic types are:

- Radial Flow: the discharge pressure is developed wholly by centrifugal force. The fluid is discharge perpendicular to the pump shaft.
- Axial Flow: the discharge pressure is developed by the lifting action of the vanes of the impeller on the fluid. Usually the fluid is discharged parallel to the pump shaft.
- Mixed Flow – most common type of centrifugal pump where the discharge pressure is developed by a combination of the centrifugal force and lift generated by the vanes of the impeller on the fluid. Fluid discharge is usually perpendicular to the pump shaft.

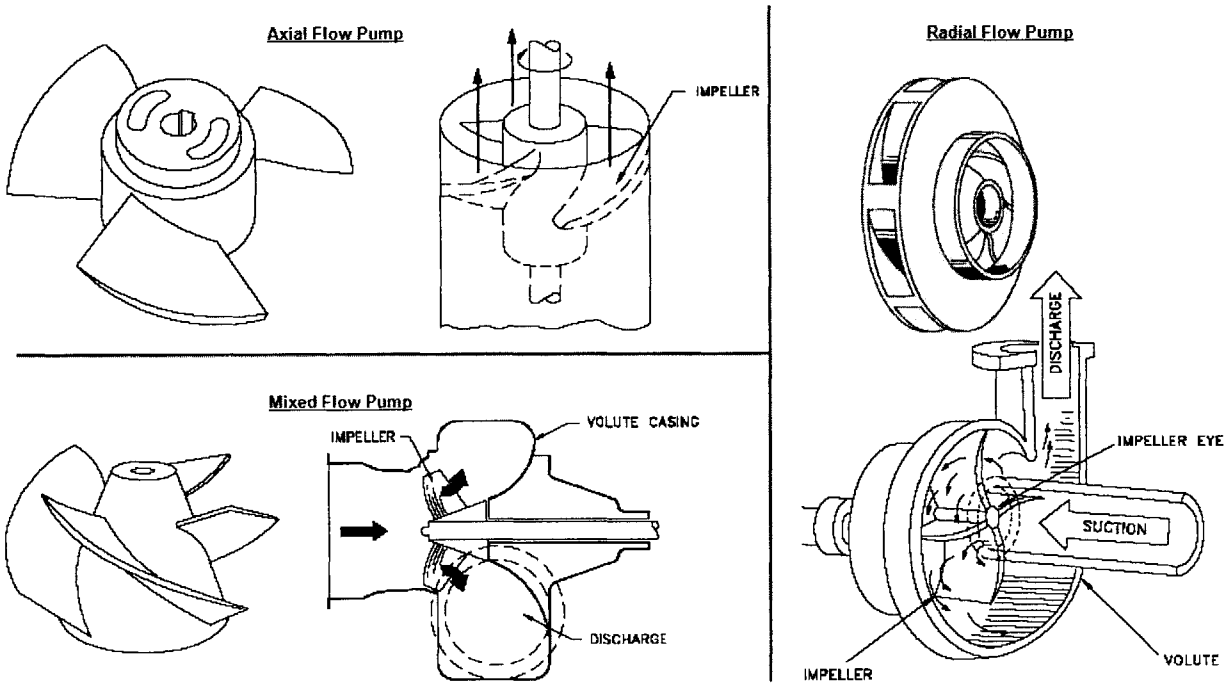

Figure 2-2: Centrifugal Pump Categories with Impeller Details [13]

2.2.2 *Positive Displacement Pumps*

Unlike centrifugal pumps, positive displacement pumps discharge a constant flow rate regardless of outlet pressure. The reciprocating pump is the most common form of positive displacement pump. This type of pump moves fluids by means of a plunger or piston that reciprocates inside a cylinder [12]. Each plunger stroke displaces a constant volume of fluid; several plungers arranged in series can achieve very high discharge pressures. Since a positive displacement pump works independently of the outlet pressure, a relief or regulating valve is required to control the system pressure.

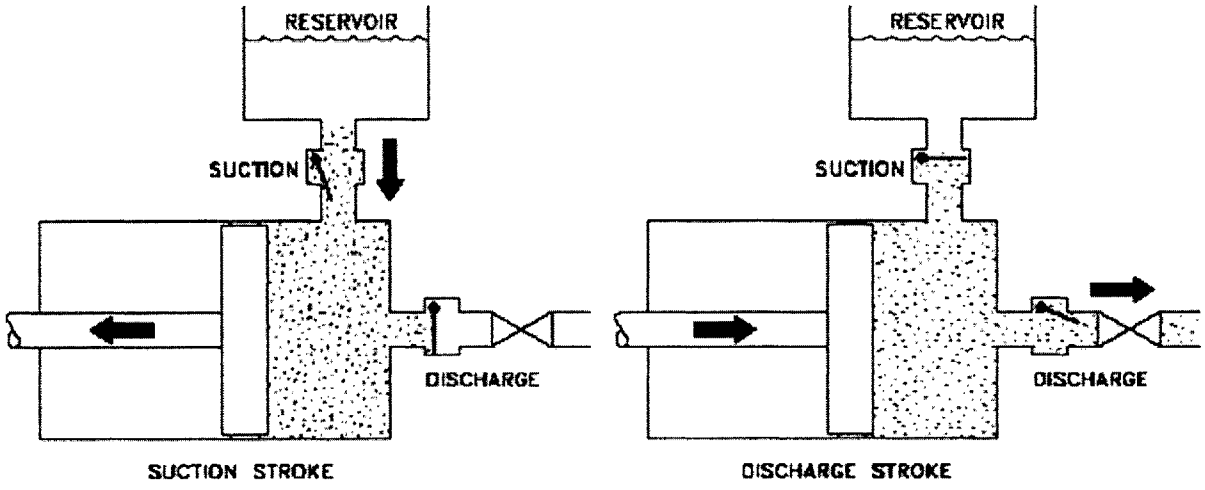

Figure 2-3: Plunger Type Positive Displacement Pump Operation [13]

2.2.3 *Filters and Membranes*

Filters and membranes remove solids and impurities from a fluid. They are usually installed on systems where foreign matter can adversely affect performance, such as the suction side of pumps. Typically, debris is separated by straining the fluid through a tight mesh, only allowing the smallest particles to pass. Membranes are used to remove molecule-sized matter. A filter or membrane cleanliness is relative by the fluid pressure drop, or differential pressure, between the inlet and outlet of the housing. Generally, a new filter will have a lower differential pressure then a fouled one.

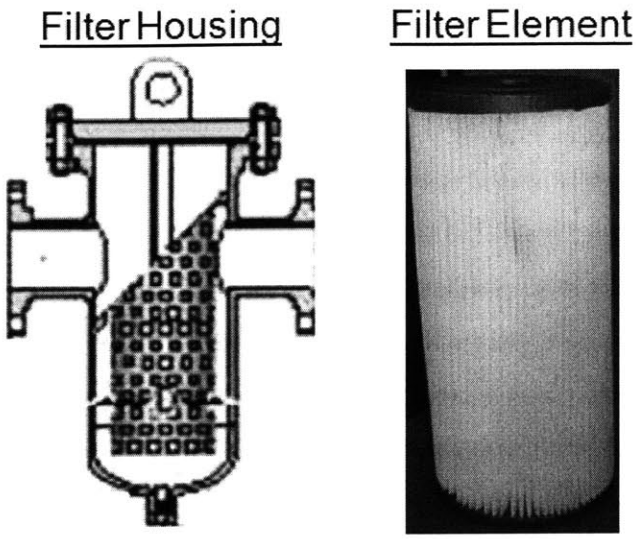

Figure 2-4: Basket Type Filter Housing and Element [13]

2.3 RC7000 Plus Reverse Osmosis (RO) System

Most ships utilize one of two techniques to produce potable water from seawater. One method is to distill the seawater by boiling it to produce steam. The steam is condensed and collected as potable water. Unfortunately, the evaporator required for this technique is energy intensive and difficult to operate. The other method is to force seawater through a semi-permeable membrane to separate particles from the pure solution. This technique, known as Reverse Osmosis (RO), is becoming the dominant potable water production method onboard ships. Simplified operations and reduced maintenance account for the increased use of electric powered RO units. In fact, starting in 2003, the U.S. Coast Guard began a program to replace the evaporator distilling plant onboard the 270-foot Famous Class Medium Endurance Cutters (WMEC) to electric driven RO units. The following sections discuss this system and the NILM installation.

2.3.1 Reverse Osmosis Process

Osmosis is a naturally occurring phenomenon in which a semi-permeable membrane separates a pure and a concentrated solution (a semi-permeable membrane is a membrane that will selectively pass some atoms or molecules but not others). The process is easily observed by

placing an egg into a bowl of water and watching it "swell" up over time. Every fluid has an inherent potential that is directly related to the type and amount of solids in solution.

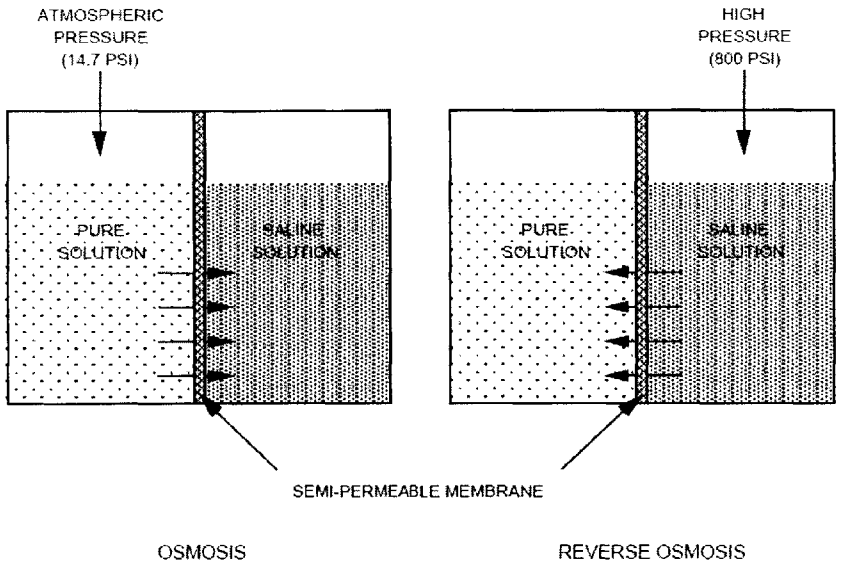

Figure 2-5: The Osmotic System [14]

In an osmotic system, shown in Figure 2-5, the less concentrated solution will attempt to equalize the concentrations of both solutions by migrating across the semi-permeable membrane. When enough pure solution migrates across the membrane such that the inherent potential difference between the solutions in no longer higher than the osmotic pressure of the membrane, the purer solution will stop flowing [14]. Reverse Osmosis is achieved by raising the pressure on the concentrated solution to hydraulically force it against the semi-permeable membrane. This only permits the pure solution to pass. The pressure required to achieve this condition is approximately 800 to 1,200 psi [15].

2.3.2 Reverse Osmosis System Description and Operation

This reverse osmosis system installed on the USCG's Medium Endurance Cutters consists of a low-pressure centrifugal pump, a 20 and a 5 micron filter in series, high-pressure positive displacement pump, semi-permeable membranes, and a high-pressure regulating valve. Figure 2-6 illustrates the arrangement of the Village Marine Tec RC7000 Plus Reverse Osmosis (RO) Unit (a detailed OEM line drawing is available in Appendix A). Note that after the low-pressure

pump the RO unit splits into two halves, referred to as "A" and "B" sides, which operate independently of each other. Table 2-2 provides component details.

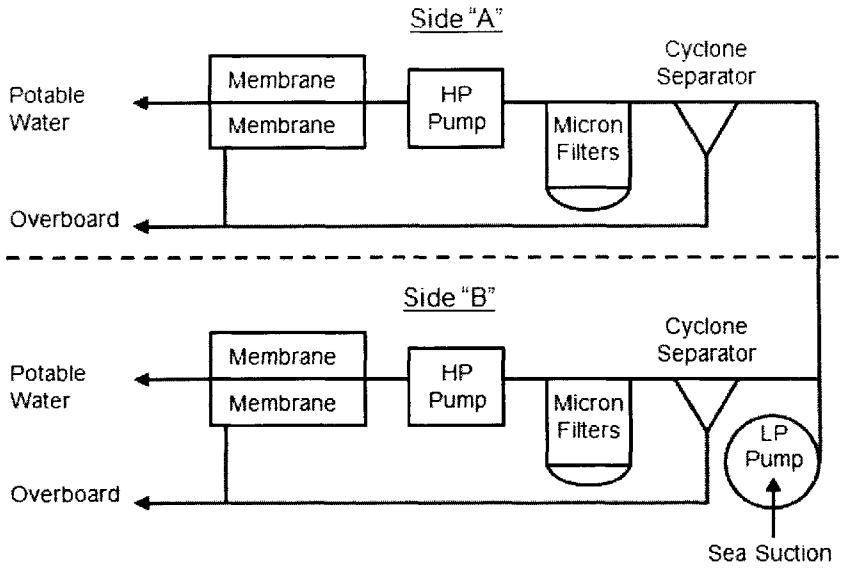

Figure 2-6: Simplified Diagram of the RC7000 Plus RO Unit

Table 2-2: RC7000 Plus RO Unit Component Details

Component	Manufacture, Model	Description
LP Pump Motor	Baldor, JMM7072T	5-Hp 3∅ AC Motor, 460V/6A, 3450 RPM
LP Pump	AmpCo, KC2	Centrifugal Pump
Cyclone Separator	VMT, CS3000-7000	Removes particles with a specific gravity of >2.7 and a diameter of >6 microns
Micron Filter	VMT, 33-2100/5100	20 and 5-micron filters remove debris from feed water
HP Pump Motor	Baldor, VM2334T	460/24, AC Motor, 3∅, 1760 RPM, 20 Hp
HP Pump	Aqua-Pro Pumps, 5P50	5 Plunger, Positive Displacement Pump
Membrane	Aqua-Pro, SW-6040	Separates NaCl from the feed water

Raw seawater from the sea-suction strainer is forced through the cyclone separator and micron filters by a 5 Hp centrifugal pump, known as the low-pressure (LP) pump. The cyclone separator discharges large suspended solids from the raw seawater while the filters trap the remaining smaller debris. The high-pressure (HP) positive displacement pump increases the pretreated raw seawater, known as feed water, pressure from 40 psi to over 800 psi. The HP pumps achieve this

by using a series of five ceramic plungers with decreasing cylinder diameters. The pressurized feed water then flows directly into the membrane array. The membrane array is a fixed arrangement of two fiberglass pressure vessels that each contain two Model SW6040 RO membrane elements that are 6" in diameter and 40" in length [14]. Reverse osmosis occurs as the semi-permeable membranes separate the pressurized feed water into two streams; the high purity product stream, referred to as permeate, and the concentrated reject stream, referred to as the brine [14]. The brine is piped directly overboard while the permeate is sent to the potable water storage tanks. Figure 2-7 shows RC7000 Plus RO Unit layout.

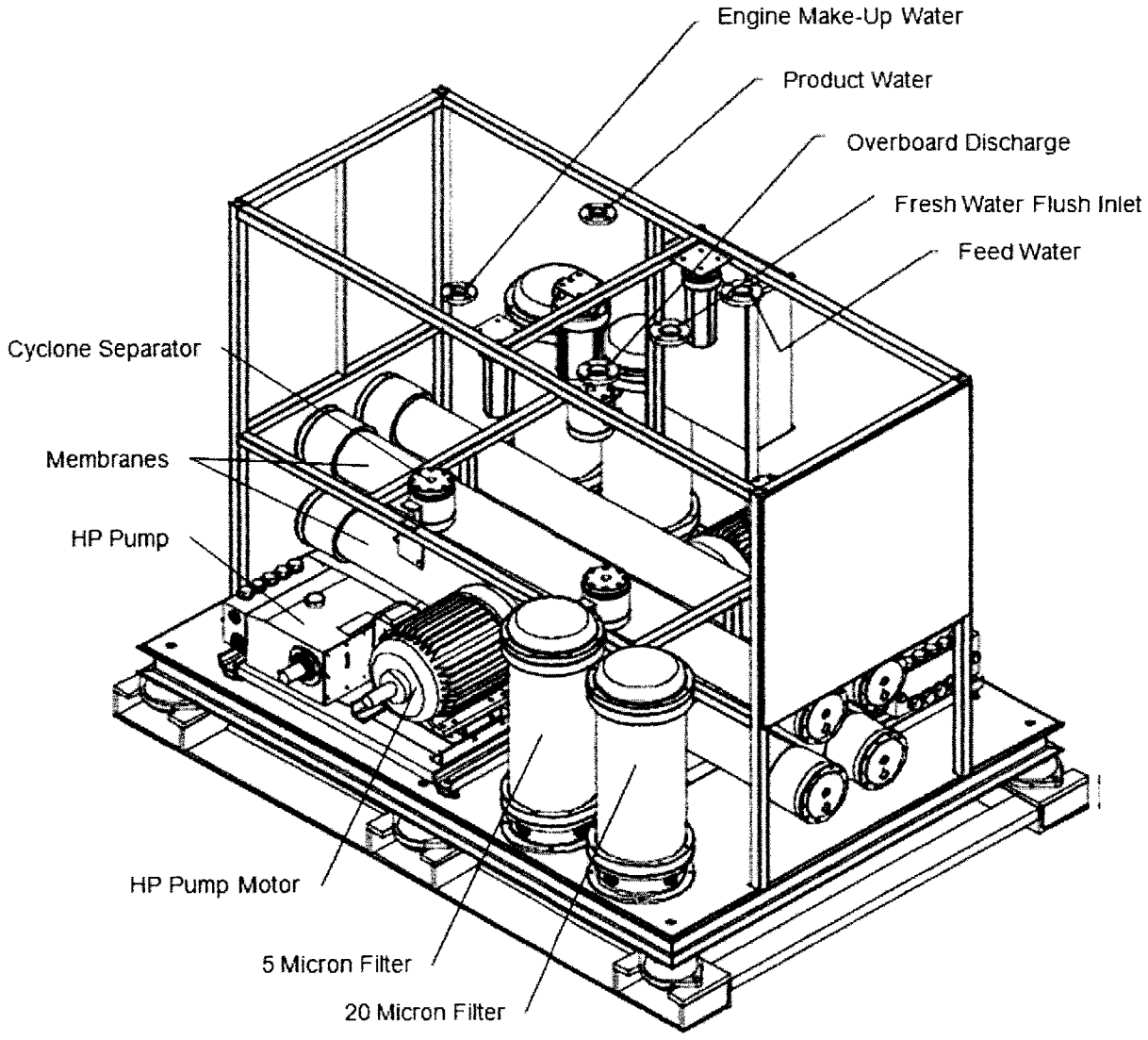

Figure 2-7: RC7000 Plus Reverse Osmosis Unit Layout [14]

There are several key valves used during normal RO operations. The following valve and component numbers are found in the detailed drawing provided as Appendix A and reference [14]. The HP Regulating Valve (valve number V6 "A/B") sets the pressure inside the membranes. Due to the high operating membrane pressure, the HP pump normally starts in an unloaded condition by using the HP Bypass Valve (valve number V7 "A/B"). This valve diverts the discharge from the HP pump overboard without going through the HP Regulating Valve, thus reducing the membrane pressure. Once the HP pump is running smoothly, it is gradually loaded by manually closing HP Bypass Valve. The Product Water Solenoid Valve (valve number V10 "A/B") automatically directs permeate to the potable water storage tanks (valve open) or overboard (valve closed) based on the product salinity measured by the Water Quality Monitor (component number MON "A/B").

2.3.3 Reverse Osmosis System NILM Installation

The RO unit NILM was first installed on the U.S. Coast Guard Cutter *Seneca* by LT DeNucci [6] in 2005 for initial data collection. In April 2006, the NILM installation was modified to collect voltage and current transducer (CT) measurements from the LP pump and "A" side HP pump on four separate channels. Originally, the data collection was split between two computers, one for the LP pump data and the other for the "A" side HP pump. A software modification in June 2006 allowed six channels, enough to cover the LP pump and two HP pumps, to be recorded by a single computer. This enabled accurate time-synced data collection, simplifying the analysis process.

In September 2006, a similar six-channel setup was installed on the U.S. Coast Guard Cutter *Escanaba's* RO unit. The only major difference was the use of channels 5 and 6 to measure the aggregate voltage and current demand to all three pumps. This was done to verify NILM's ability to monitor multiple loads from a single pair of voltage and current measurements. Unfortunately, during the first two months of data collection over 50% of the hourly snapshots were missing or incomplete. The cause of the problem was isolated to a combination of reference voltage loss while the RO unit was secured and an overloading of the transfer rate between the PCI-1710 card and PC hard disk during prolonged 48,000 Hz data collection (i.e. 8,000 Hz per channel). Software modifications made in November 2006 resolved both issues.

The current *Seneca* RO Unit NILM configuration was made in December 2006. The software and hardware were set to record a single voltage and current channel pair for the aggregate pump loads, allowing the computer's hard drive to store three times as many hourly snapshots before reaching capacity. The *Escanaba* received the same modification in January 2007. Table 2-3 and Table 2-4 outline the components and settings used for each NILM configuration.

Table 2-3: *Seneca* NILM Setup

	Channel	Component	Resistance	Gain	Data
20060618-20061216	1	B-C Voltage	100Ω	0	Raw
	2	*i*-A LP Pump, CT: LA-100P	49.9Ω	1	
	3	B-C Voltage	100Ω	0	Raw
	4	*i*-A HP-A Pump, CT: LA-305S	49.9Ω	0	
	5	B-C Voltage	100Ω	0	Raw
	6	*i*-A HP-B Pump, CT: LA-305S	49.9Ω	0	
20061216-Present	1	A-B Voltage	100Ω	0	Raw
	2	*i*-C 3-Pump Aggregate, CT: LA-150S	30.1Ω	0	

Table 2-4: *Escanaba* NILM Setup

	Channel	Component	Resistance	Gain	Data
20060918-20070126	1	A-B Voltage	100Ω	0	Raw
	2	*i*-C LP Pump, CT: LA-100P	100Ω	0	
	3	A-B Voltage	100Ω	0	Raw
	4	*i*-C HP-A Pump, CT: LA-150S	30.1Ω	0	
	5	A-B Voltage	100Ω	0	Raw
	6	*i*-C 3-Pump Aggregate, CT: LA-150S	30.1Ω	0	
20070126-Present	1	A-B Voltage	100Ω	0	Raw
	2	*i*-C 3-Pump Aggregate, CT: LA-150S	30.1Ω	0	

Figure 2-8 depicts the *Escanaba* RO unit's power panel with the NILM installation. The voltage and current transducers (CT) connect to the NILM and data collection computer by way of category 5 cable leads through the bottom of the power panel.

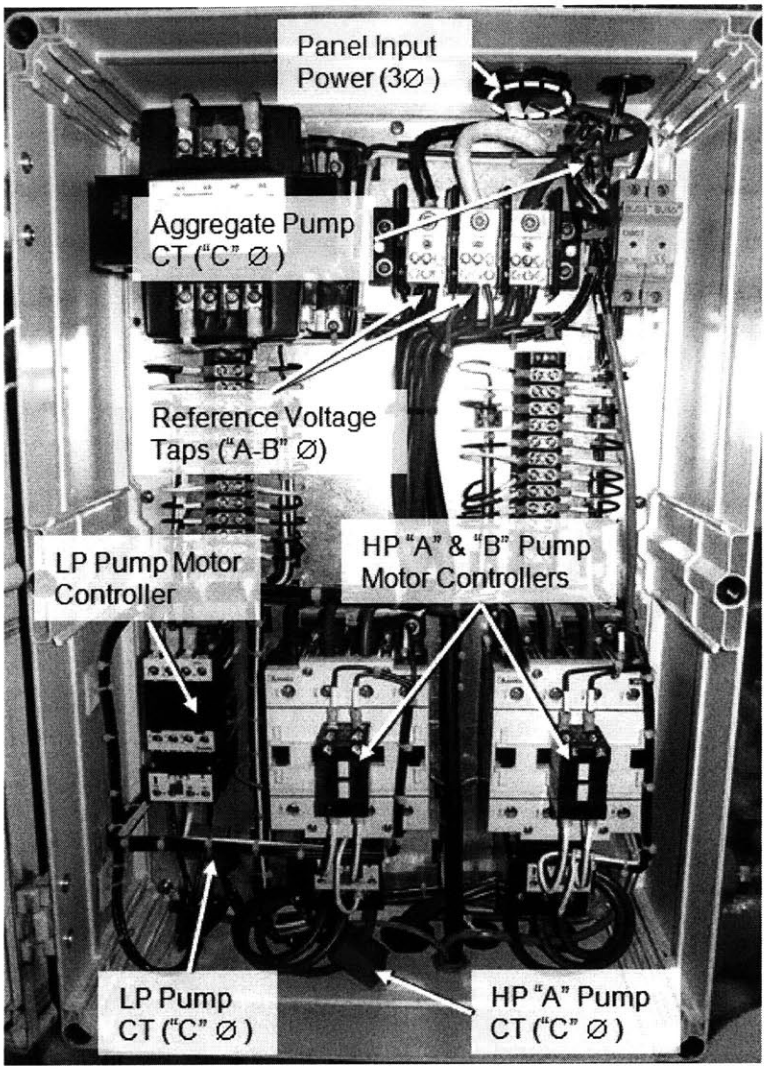

Figure 2-8: The *Escanaba*'s RO Unit Power Panel with the NILM Installation

2.4 Laboratory Test Stand

To facilitate a controllable environment for conducting fluid pump and filter experiments a laboratory test stand was constructed. The test stand enabled a quick succession of experiments to explore and corroborate field data while increasing system understanding.

2.4.1 Laboratory Test Stand System Description

The laboratory test stand is composed of a reservoir, centrifugal pump, three phase AC motor, filter housing, and piping network. A flowmeter, tachometer, and two differential pressure gauges in conjunction with a NILM attached to the AC motor measure and record system

properties. Figure 2-9 provides a detailed system diagram of the laboratory test stand. Component and sensor details are available in Table 2-5.

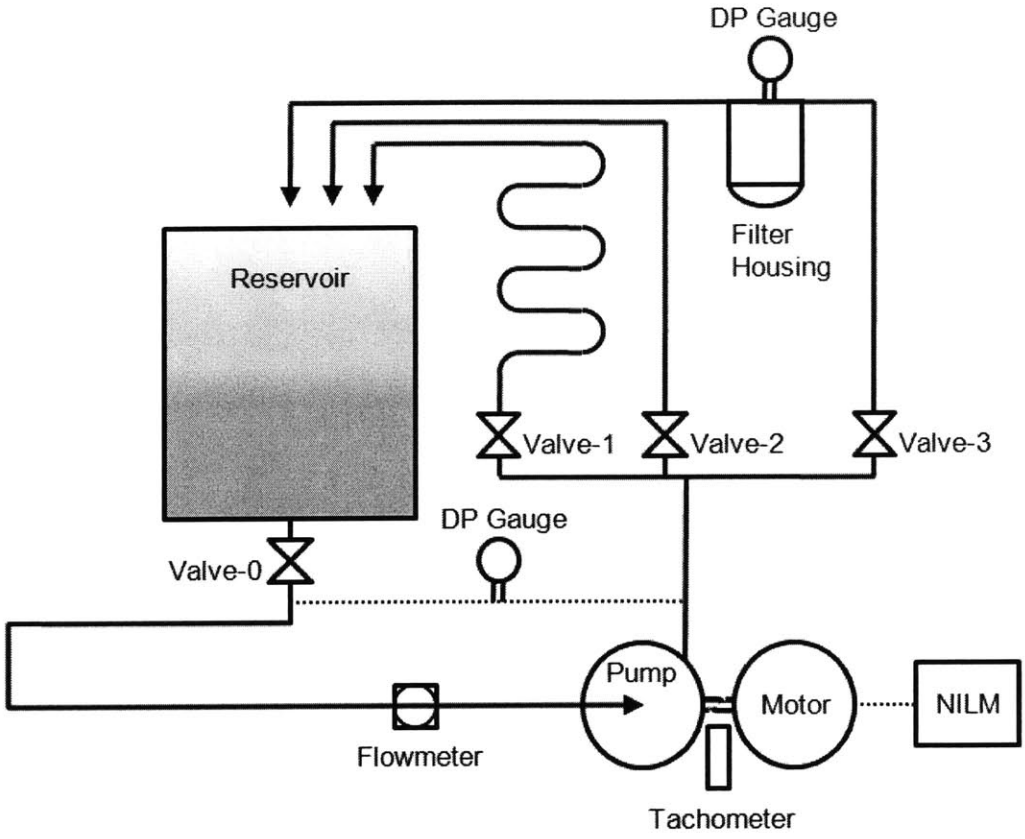

Figure 2-9: Laboratory Test Stand System Diagram

Table 2-5: Laboratory Test Stand Component Details

Component	**Manufacture, Model**
Centrifugal Pump	Sherwood, COP-BB5
AC Motor, 3∅, 3450 RPM	GE, K156
NILM	(see **Table 2-6**)
Filter Housing	GE, GXWH35F
Filter Element	GE, FXHSC
Flowmeter	Omega, FP7001A
Tachometer	Monarch Instruments, ROS-W25
Differential Pressure Gauge	SETRA, 230

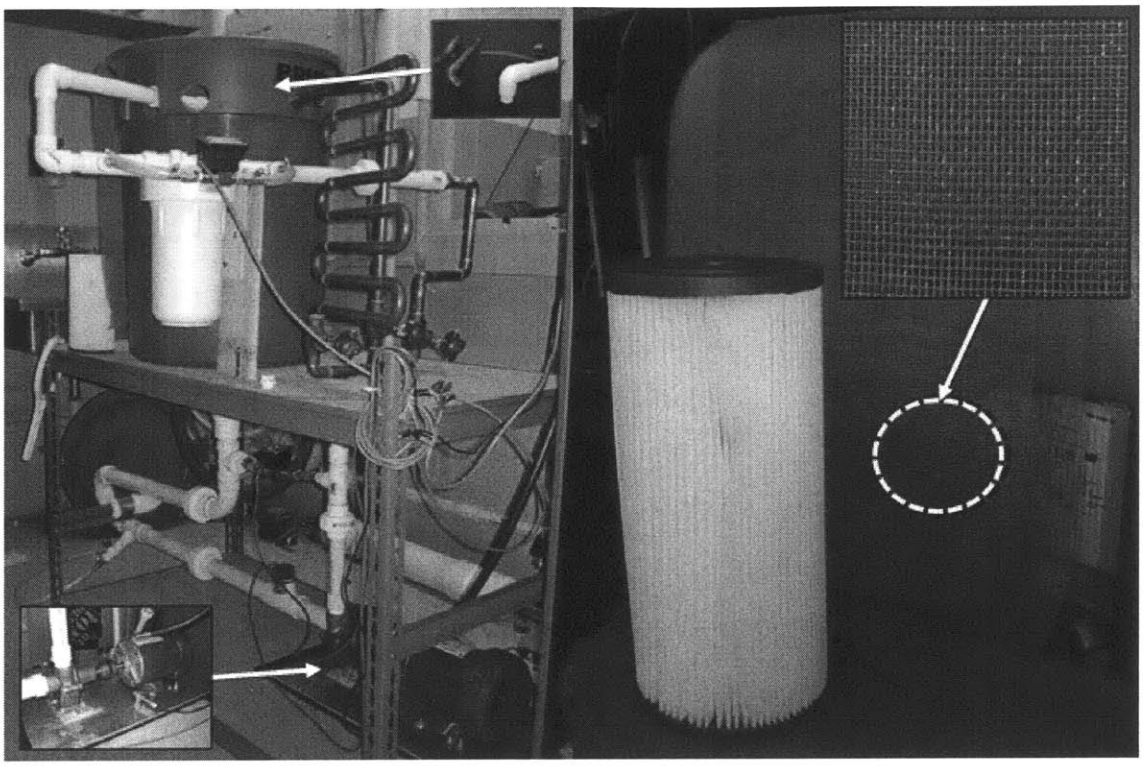

Figure 2-10: Photographs of the Laboratory Test Stand, Filter Element, and Fouling Screen

2.4.2 Laboratory Test Stand NILM Configuration

The ultimate purpose of the laboratory test stand is to correlate measurable fluid system properties with the pump motor power demand and transient characteristics. Table 2-6 provides the NILM configuration used for laboratory experiments.

Table 2-6: Laboratory Test Stand NILM Configuration

Channel	Component	Resistance	Gain
1	B-C Voltage	100Ω	2
2	*i*-A Current Transducer, LA-55P	100Ω	2
3	C-A Voltage	100Ω	2
4	*i*-B Current Transducer, LA-55P	100Ω	2
5	Pump DP Gauge	49.9Ω	2
6	Flowmeter	-	0
7	Tachometer	-	0
8	Filter DP Gauge	110Ω	2

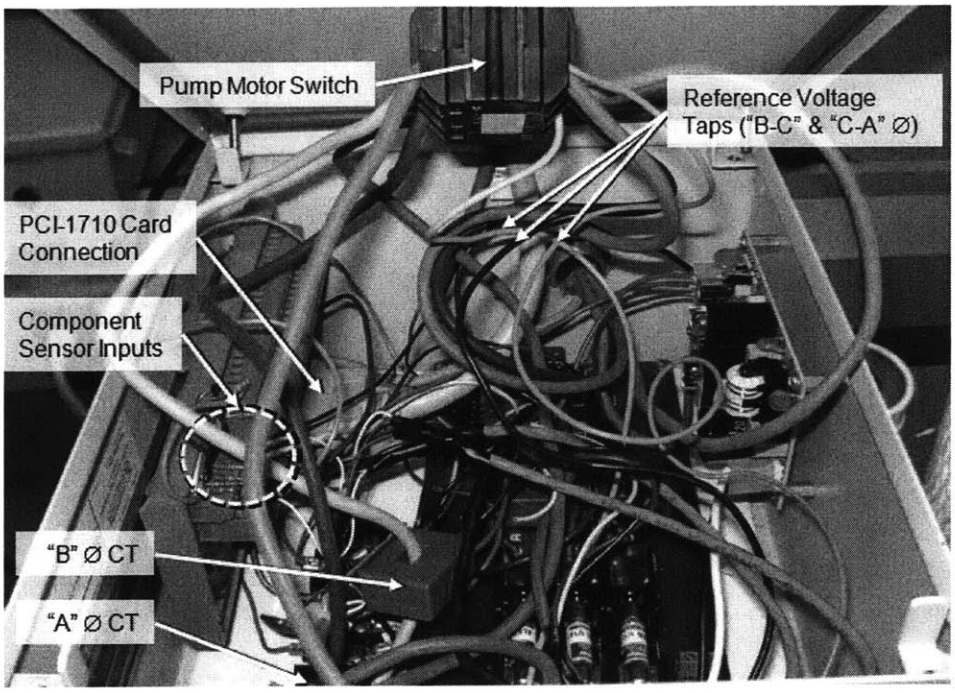

Figure 2-11: Laboratory Test Stand NILM Setup

The flowmeter and tachometer are square wave pulse generators where the time between up-crossings is the cycle period. One cycle from the tachometer represents one revolution of the pump motor shaft. Dividing a single cycle by its period calculates instantaneous pump shaft RPM. One cycle from the flowmeter is a complete revolution of the sensor paddle wheel in the pipe flow stream. For a 1.5-inch diameter PVC pipe, 29.46 cycles equates to 1 gallon flowing past the sensor. Equation 2.4-1 converts the flowmeter cycles to gallons per minute (GPM) for an 8,000 Hz data collection rate.

$$GPM = \frac{8000 \cdot 60}{K_{factor} \cdot C_{crossing}} \tag{2.4-1}$$

Where: GPM = flow rate through test stand pump (gal/min)
K_{factor} = flowmeter calibrated value provided by manufacture (29.46 cycles/gal)
$C_{crossing}$ = bits between up-crossings

To convert the SETRA differential pressure transducer output to a pressure value the A/D converter output voltage data from channels 5 and 8 must be scaled for a range of -5 to +5 volts.

Since the A/D converter quantizes data into values that range between 0 and 4096, Equation 2.4-2a provides the appropriate conversion [6].

$$V_{SETRA} = \frac{10}{4096}(D_{SETRA} - 2048) \tag{2.4-2a}$$

Where: V_{SETRA} = measured transducer voltage (Volts)
D_{SETRA} = recorded transducer data

Dividing the transducer voltage by the value of the measuring resistor the sensor output current is found, as shown in Equation 2.4-2b.

$$I_{SETRA} = \frac{V_{SETRA}}{R_{SETRA}} \tag{2.4-2b}$$

Where: I_{SETRA} = measured transducer current (Amps)
V_{SETRA} = measured transducer voltage (Volts)
R_{SETRA} = measuring resistor size (Ohms)

Finally, the differential pressure, in pounds per square inch (psi), is determined using Equation 2.4-2c [16].

$$DP_{SETRA} = \frac{50(I_{SETRA} - 0.004)}{0.016} \tag{2.4-2c}$$

Where: DP_{SETRA} = measured transducer differential pressure (lbs/in^2)
I_{SETRA} = measured transducer current (Amps)

Figure 2-12 provides the measured pump curves for the laboratory test stand. The pump curves were generated by measuring the flow rate through the pump at various pump speeds and system heads. The pump speed was set using a variable speed drive (VSD) to alter the pump motor RPM, while PVC pipe attachments with different outlet heights provided different system operating heads.

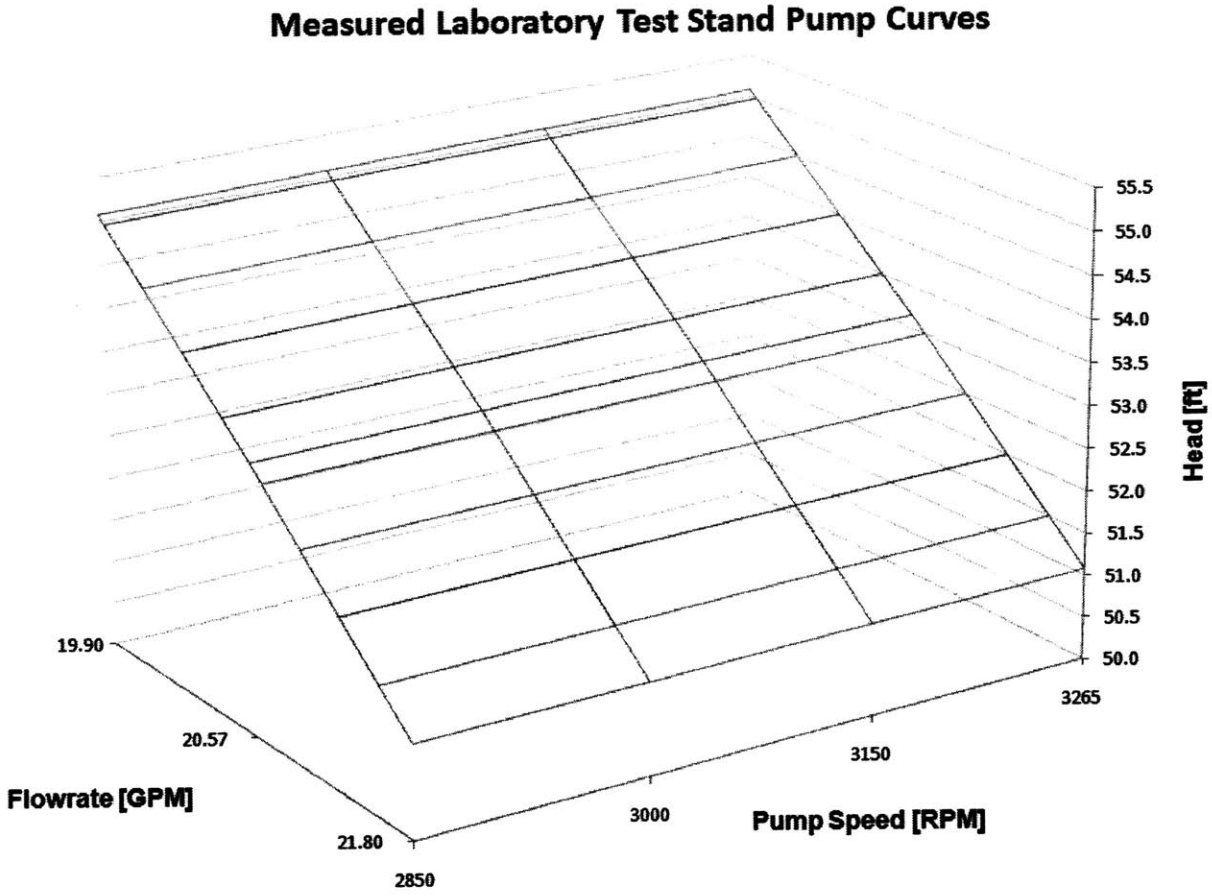

Figure 2-12: Measured Laboratory Test Stand Pump Curves

3 Basic Fluid System Diagnostic Indicators

The following chapter reviews events and conditions recorded by the NILM while monitoring the RO units on the U.S. Coast Guard Cutters *Seneca* and *Escanaba* over the past year.

3.1 System Status Determination

One of the most observable NILM applications is determining the system status and alignment. An "on" or "off" assessment is the first step in system monitoring, but as the following sections illustrate many other system properties are easily evaluated from the power demand traces.

3.1.1 Pump Starts and Stops

With three pumps, the RO unit can have a significant range in power demand and on/off sequencing. As shown in Figure 3-1, the NILM can determine the pump status by simply measuring the power demand.

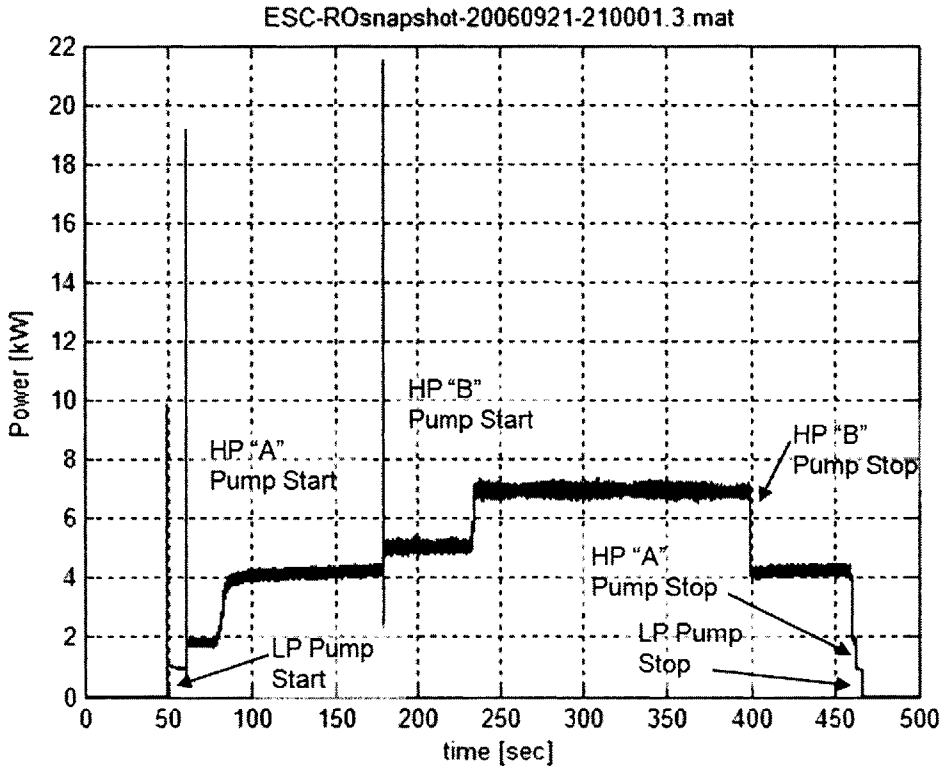

Figure 3-1: RO Unit Pump Starts and Stops

An interesting feature present in the HP pump start is what appears to be an overshoot from an under-damped system as highlighted in Figure 3-2. Review of multiple HP pump starts indicates that the overshoot is a characteristic of the system. As the HP pump is connected to the motor by v-belt drive, as shown in Figure 3-14, this type of behavior is expected due to the belt's elastic properties. A detailed analysis was not conducted for this particular feature, but similar to the ASW pump coupling failure discussed in LT DeNucci's thesis [6], it could certainly lead to a diagnostic indicator.

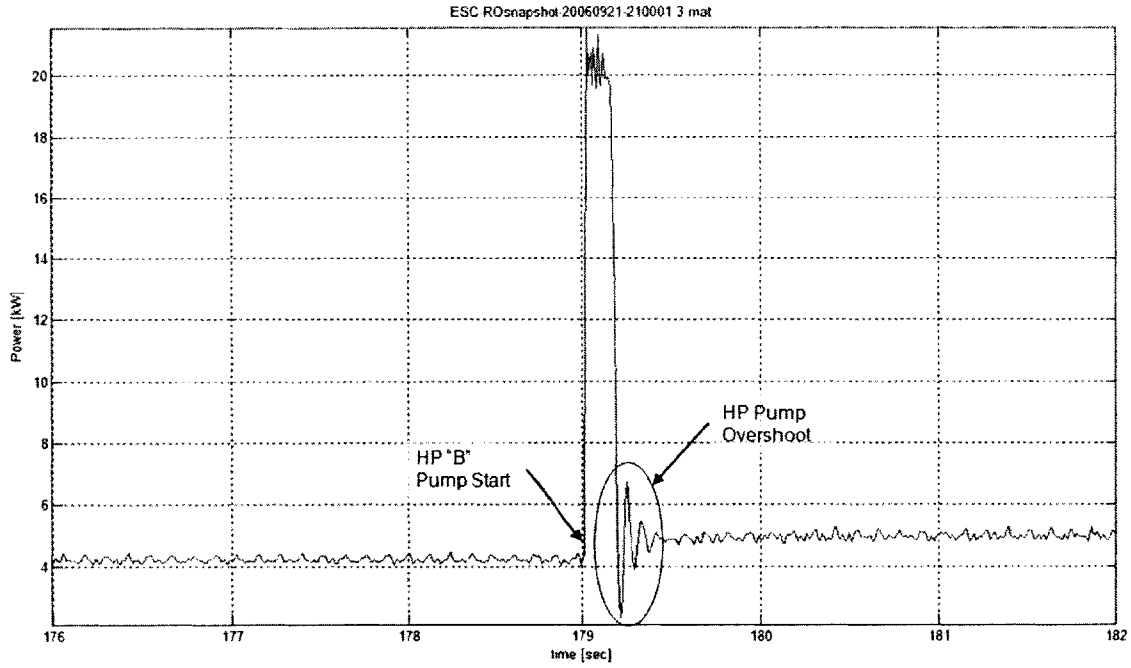

Figure 3-2: Detail of HP "B" Pump Start from Figure 3-1

By tracking the pump statuses NILM is able to record the accumulated running time for each system component and alert the operator of time driven preventative and routine maintenance items.

3.1.2 Valve Alignment Changes

In addition, the aggregate real power trace reveals valve alignment changes that affect the pump load. As shown in Figure 3-3, when the high-pressure bypass valve (V7 "A/B") is closed the power demand to the HP pump increases. Valve number V7 bypasses the membrane pressure-regulating valve so that the HP positive displacement pump initially starts in an "unload"

condition. As the valve closes the internal membrane pressure increases causing the HP pump to demand more power. In some cases watchstanders start the HP pump with valve number V7 closed placing a tremendous amount of friction and stress on the ceramic plungers. Additionally, the sudden increase in membrane pressure could damage the seals, leading to leaks and failures. This practice will shorten the pump life and increase the RO unit's maintenance needs.

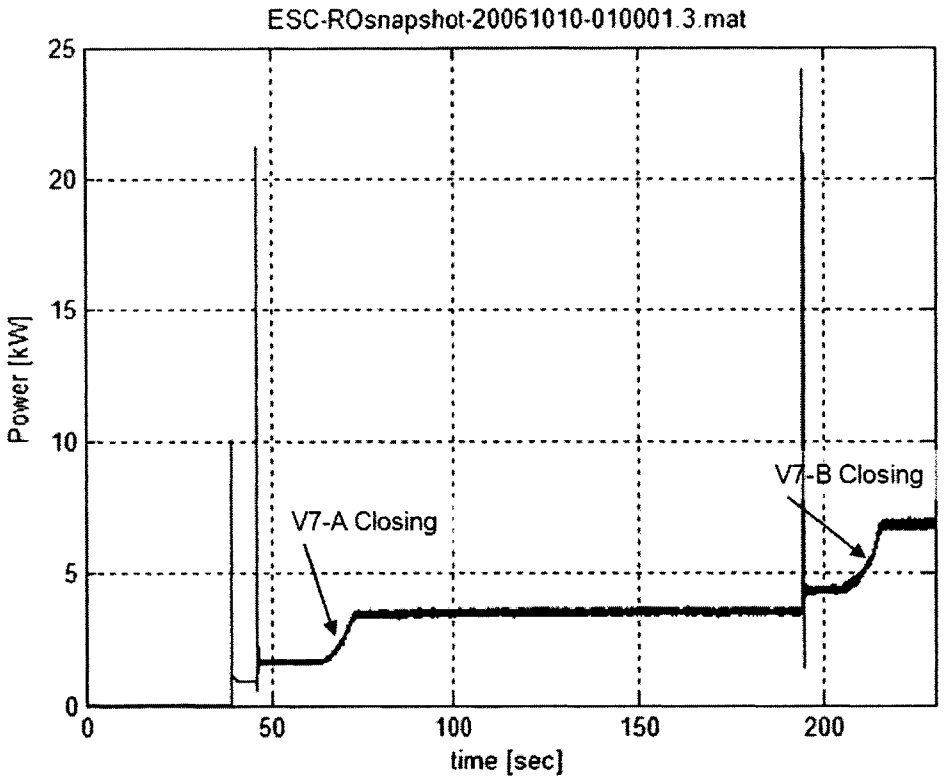

Figure 3-3: RO Unit Major Valve Alignment Changes

Presently, there is no interlock to prevent incorrect operation of the bypass valve, but looking at the real power demand difference between the open and closed valve positions it is clear that NILM could detect this condition. With a connection between the NILM and the master control consol, a detected HP pump start with the bypass valve closed could trigger the solenoid trip valve already installed on the system, lowering the initial membrane pressure and pump loading.

3.1.3 RO System Start Sequence

Like most complex systems, the RO unit has a specific start procedure to minimize damaging conditions during activation process. Using the "Normal Start-Up Procedure" outlined in

Section 4.2 of the *RC7000 Plus Manuel* [14] it is easy to follow and verify a successful start sequence from the NILM power trace as shown Figure 3-4.

Section 4.2, Steps 4 through 6:

4) Start the LP boost pump by depressing the *LP Pump pushbutton* located on the MCC.

5) Start the HP pump unit by depressing the *HP PUMP Pushbutton* located on the MCC. At least 10 psi must be indicated on the discharge side of the *Micron Filter Array Duplex Pressure* gauge.

6) When flow through the reject discharge flow meter appears to be free of air bubbles, slowly close *High Pressure Bypass Valve* (V7 A/B). It is important to monitor the pressure indicated on the Membrane Array Pressure Gauge (PG5 A/B).

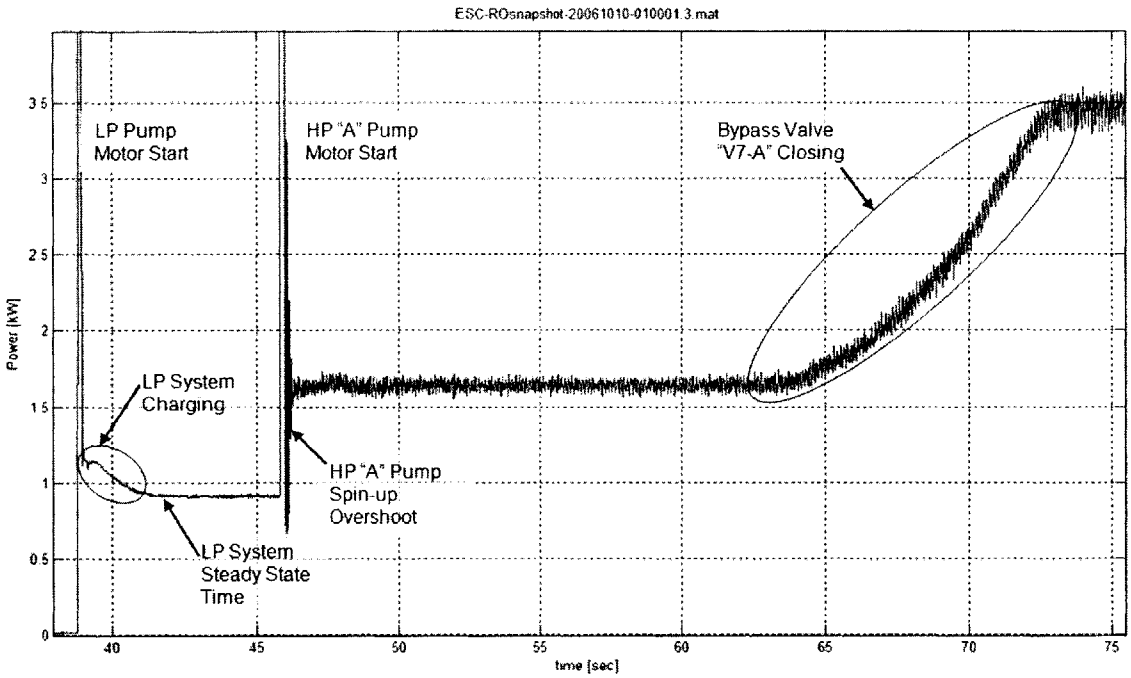

Figure 3-4: NILM Real Power Trace from Successful RO Start Sequence

Key features during a normal start sequence are identified in Figure 3-4. A common mistake made by watchstanders is not allowing the HP pump inlet pressure to come up before trying to start it. There is an interlock to prevent the HP pump from starting without at least 10 psi of inlet pressure, but the interlock does not determine if the inlet pressure has stabilized. Starting the HP pump before the inlet pressure has stabilized increases the likelihood of damage to the pump due to unsteady flow and pressure oscillations. From the real power trace, the NILM can determine when the pressure has stabilized by checking the LP pump power differential over time. When

the differential goes to zero, as indicated at 42-seconds in Figure 3-4, the LP pump has reached steady state and it is safe to start the HP pump.

A simple NILM diagnostic tool would evaluate the *correctness* of each start by comparing it to a known baseline start. In doing so, the NILM could alert the watchstander of possible problems or system misalignments, thus mitigating the harmful effects of improper equipment operation before it causes severe damage.

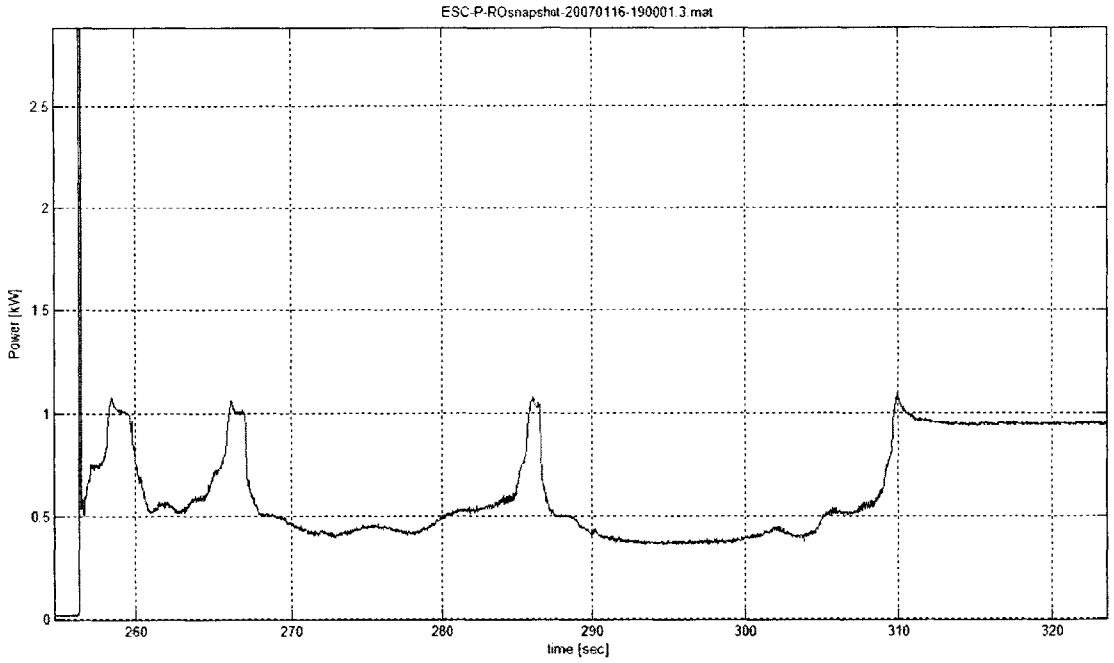

Figure 3-5: An Air Bound LP Pump Start

Figure 3-5 is an example of a faulty RO unit start, where the LP pump was air bound as indicated by the sporadic power demand. After the initial start this condition was allowed to continue for nearly 60 seconds before the system was properly vented. Using NILM to monitor the RO unit start sequence could have alerted the watchstander of the possible problem and minimize exposure to the pump damaging condition.

3.2 Maintenance Indicators

Field tests have demonstrated the NILM's ability to detect conditions that precede serious pump failures. Examples include abnormal operation in highly contaminated waters and large oscillations in the steady-state power drawn by pump motors. Other indicators include spectral content within the power demand that, when trended, provide a real-time measure for condition based maintenance.

3.2.1 Abnormal Event Detection

An analysis of the NILM data collected from the *Escanaba* and *Seneca* reveals a wide range of RO unit operating conditions. It would be inefficient to develop an algorithm capable of diagnosing every damaging condition the RO unit might experience. A more practical approach would have the NILM monitor the power demand and its spectral content for characteristics that exceed baseline parameters. The following sections examine several damaging situations where it is clear that a simple abnormal event detection algorithm could immediately alert the watchstander of detrimental operating conditions, enabling them to take action and mitigate the effects.

3.2.1.1 Multiple Pump Restarts

Contamination can have a catastrophic effect on the positive-displacement pumps in the RO system. It is well known that RO units are to be secured before entering harbors or other regions that would overload the system's pretreatment capabilities (i.e. the micron filters). Occasionally, however, the crew may not be aware that the vessel has entered a region that may cause problems. If that happens, the pressure across the micron filters can increase, thus reducing the pressure at the inlets to the positive-displacement pumps. As a precaution, the controller is designed to secure the high-pressure pumps whenever their inlet pressures fall below a certain threshold. If the pump inlet pressure fluctuates, however, the pump may experience multiple restarts. Such activity usually goes unnoticed because manual inspections are performed only periodically.

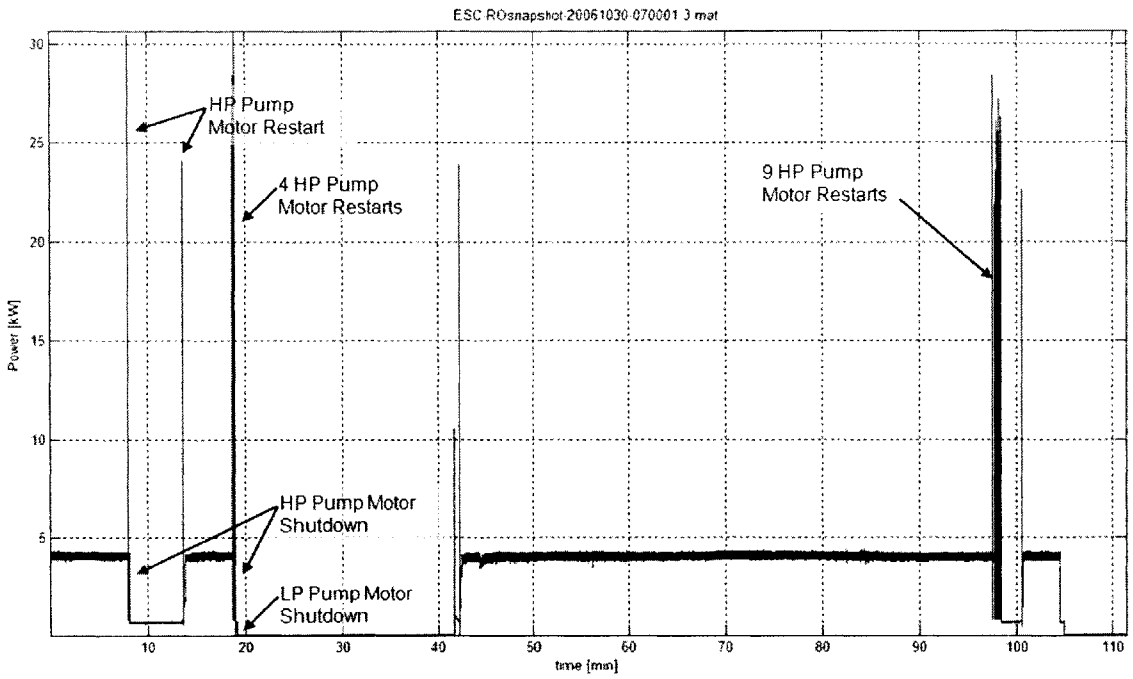

Figure 3-6: Multiple HP Pump Restarts

Figure 3-6 shows the aggregate pump power drawn by RO unit during a period when the *Escanaba* was passing through contaminated waters. Initially, the LP pump and one HP pump were operating. Shortly before minute 10, the HP pump secured, re-started, and then secured again for several minutes. During this time, the LP pump ran by itself. Around minute 14, the HP pump re-started, likely because its inlet pressure increased. Several minutes later, the HP pump secured and re-energized 4 times in less than 60 seconds. Engineering logs indicate that this behavior was noticed by a nearby operator who subsequently secured both the HP pump and the LP pump. After approximately 20 minutes, the system was brought back online, and operated normally until about minute 96. At that time the HP pump again began to progress through a series of starts and stops. Finally, nine starts were recorded during an approximately two minute interval. The HP pump remained secured until shortly after minute 100. A short while later, logs indicate that the system was secured after a watchstander noticed a high differential pressure across the micron filters. The erratic behavior of the HP pump, which is difficult for human operators to notice, was easily detected by the NILM. In this case, the NILM could have acted to alert operators or automatically secured the system preventing further component damage.

3.2.1.2 *Pump Cavitation*

The power trace of the *Seneca*'s LP pump motor, Figure 3-7, illustrates another abnormal and component damaging event captured by the NILM in September 2006. The obvious box-shaped modulation with a 30-minute period is extremely uncharacteristic of the RO system. Examining the frequency spectrum using the MATLAB® script provided in Appendix B reveals the magnitude at 29.5 Hz shifts between 6,000 and 34,500 on the "thin" and "fat" pulses. This unusual signature disappeared after 12 hours.

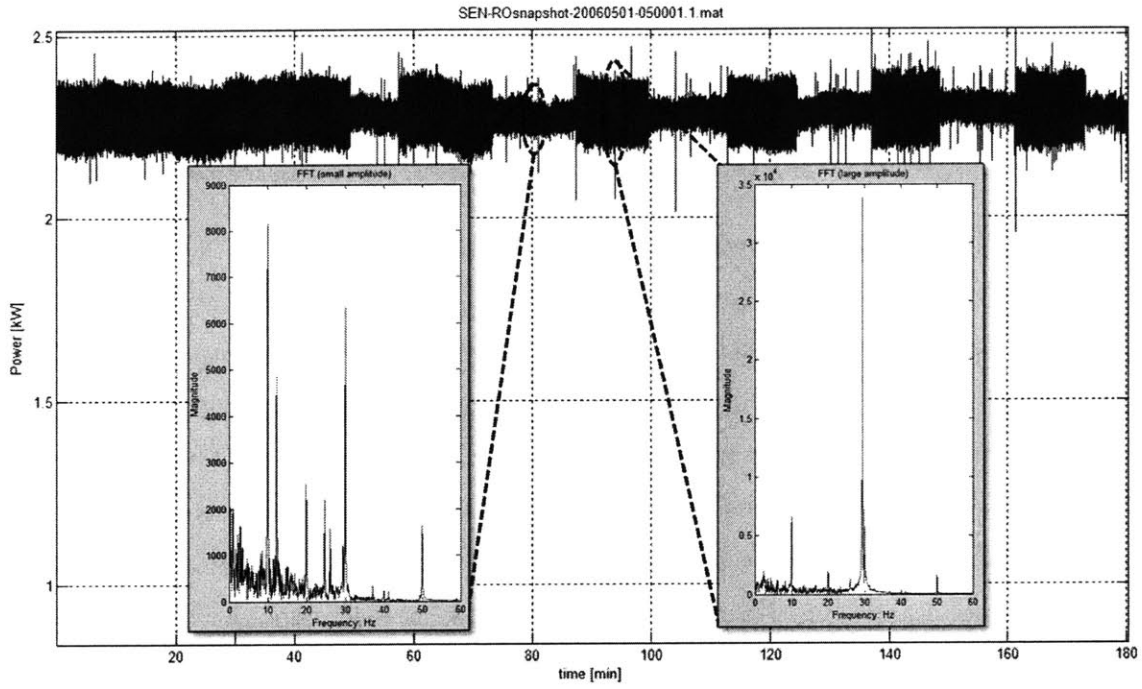

Figure 3-7: LP Pump Power Modulation

Subsequent interviews with the crew indicate that the single LP pump has difficulty supplying both the "A" and "B" sides of the RO unit if the sea suction strainers or micron filters are slightly fouled. A likely cause of the large modulation is a combination of high auxiliary seawater (ASW) system demand and a fouled sea-suction strainer. Upon tracing the seawater supply piping it was confirmed that both the RO Unit and ASW system, as shown in Figure 3-8, tap into the same sea-suction strainer. Additionally, the ship had just gotten underway the day before from a two-month inport period. After this length of time, the sea-suction strainer basket is likely fouled by marine growth if not properly cleaned.

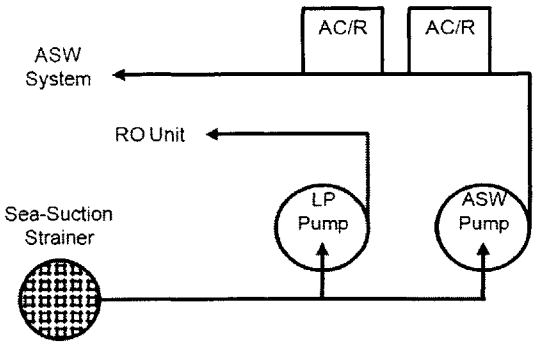

Figure 3-8: RO Unit and ASW Seawater Supply

The restricted flow rate through the fouled sea-suction strainer coupled with the high ASW demand from the air conditioning/refrigeration (AC/R) unit's 15 minute chilling cycle "starved" the RO unit's LP pump. The lower flow rate through the LP pump caused the pump inlet pressure to drop, lowering the net positive suction head (*NPSH*). Equation 3.2-1 describes NPSH available as a function of the pressure at the pump inlet minus the working fluid's saturation pressure [17].

$$NPSH_A = P_{suction} - P_{saturation} \tag{3.2-1}$$

Where: $NPSH_A$ = net positive suction head available
$P_{suction}$ = fluid pressure at pump inlet
$P_{saturation}$ = fluid saturation pressure

For a particular pump/piping system configuration a minimum NPSH, or net positive suction head required ($NPSH_R$), is needed to ensure correct pump operation. The pump will cavitate if the $NPSH_A$ falls below the $NPSH_R$ [12] [17]. Cavitation results from cavities, or bubbles, forming in the working fluid on the low-pressure, or suction, side of the pump. As the bubbles pass across the impeller, to the high-pressure side of the pump, they collapse causing noise, vibration, and impeller vane surface pitting. The suction pressure, $P_{suction}$, at the pump inlet is a combination of the static fluid head due to system elevation changes and the head losses from the pump suction piping. Other factors that can adversely affect the suction pressure are restrictions to the available flow rate caused by shared supply systems or fouled piping and strainers. Both conditions were present and likely caused the LP pump to cavitate resulting in the unusual power modulations.

Figure 3-9 provides a real power trace of the LP pump motor with the possible onset of cavitation. In this case, the cavitation was likely initiated by the diversion of the product water overboard. This RO unit configuration bypasses the semi-permeable membranes causing the HP pump discharge pressure to drop and slightly increasing the flow rate. The change in system flow rate increases the fluid velocity and reduces the pressure at the LP pump inlet ($P_{suction}$), ultimately, lowering the $NPSH_A$. As discussed previously, if the $NPSH_A$ is less than the $NPSH_R$ there is a danger of pump cavitation.

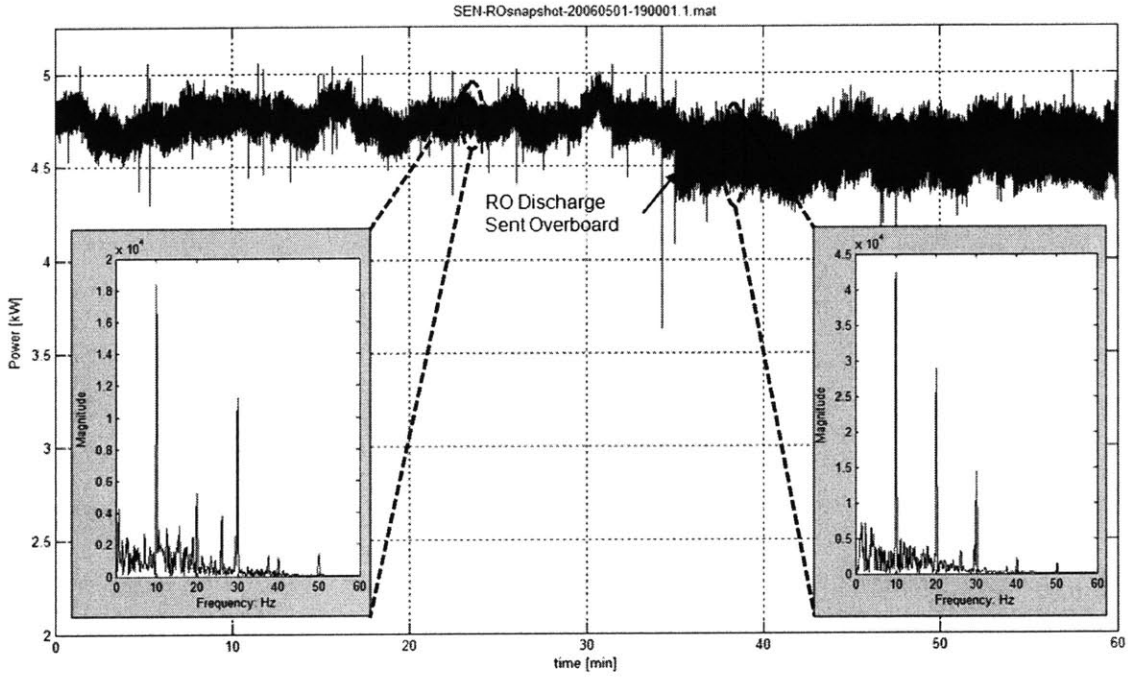

Figure 3-9: Possible LP Pump Cavitation after the Product Water was Diverted Overboard

The trace in Figure 3-9 clearly shows the real power amplitude increasing with the possible onset of pump cavitation at time 35-minutes. This time also corresponds to the overboard discharge alignment noted in the *Seneca*'s operating logs. Also, note that the average power demand decreased by 0.25 kW, from 4.75 kW to 5.0 kW, at this same point. Examining the spectral content using the code provided in Appendix B indicates a similar increase in magnitude at 9.8 Hz, 19.7 Hz, and 29.5 Hz to that identified in Figure 3-7. Unlike Figure 3-7, the dominate frequency magnitude change in Figure 3-9 occurs at 19.7 Hz where it increased from 5,500 to 30,000 between the non-cavitating and cavitating states. The magnitude at 9.8 Hz also doubles

between the two states. The difference between the telltale frequencies described in Figure 3-7 and Figure 3-9 may be attributed to the severity of the cavitation condition experienced by the respective scenarios. The situation illustrated in Figure 3-7 more severely influenced the LP pump flow rate than the one encountered in Figure 3-9. Ultimately, both figures illustrate clear changes in the LP pump motor power demand between the non-cavitation and cavitating states.

The effects of cavitation are extremely damaging to the pump impeller. Immediate impacts lower the pump's efficiency, flow rate capacity, and discharge head. Prolonged exposure can drastically increase component failures, such as shaft seals and bearings, from excessive vibration and impeller imbalances. Finally, severe cavitation over a significant period can bend, and even break, impeller vanes, ultimately destroying the pump housing.

To verify the possibility of pump cavitation the laboratory test stand was used to replicate the effects of the reduced flow rate through the pump. The fouled sea-strainer was modeled by throttling the isolation valve between the test stand reservoir and the pump inlet, identified as "Valve-0" in Figure 2-9.

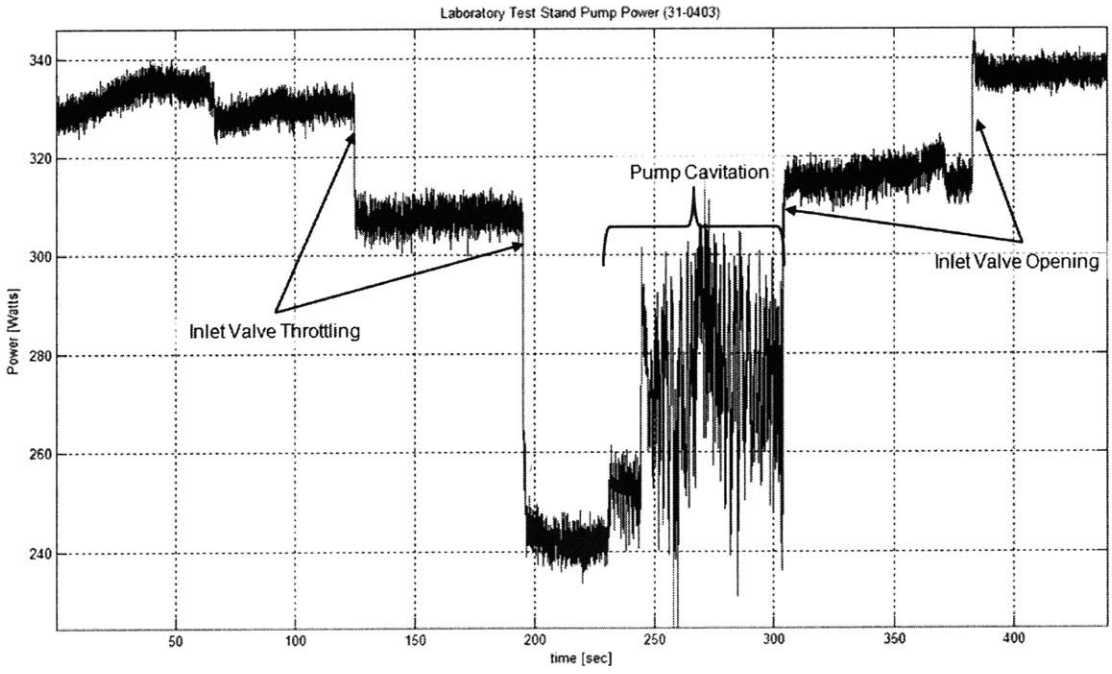

Figure 3-10: Test Stand Pump Power while Throttling the Inlet Valve

Incremental changes in the valve position slowly restricted the flow rate into the pump. As shown in Figure 3-10 the pump motor power indicates a step change between each inlet valve change. After the fourth valve change, the pump motor power amplitude gets very large, similar to the power modulation shown in Figure 3-7 and Figure 3-9. Notably the decrease in average power demand at the cavitation state found in Figure 3-10 corresponds exceptionally well to the average power demand noted in Figure 3-9. Noise caused from bubbles collapsing inside the pump detected at time 250 seconds corresponds to changes in the pump power amplitude and spectral content agree with the field observations and suggest the presence of pump cavitation.

It should be noted that the difference between a cavitating pump and an air bound pump is very slight and highly dependent on the balance of inlet and outlet pressures. The significant drop in pump power records this small window at 200 seconds in Figure 3-10. The system was extremely sensitive and a small change in valve position resulted in a significant impact on the system performance. As the valve was slowly opened between 230 and 250 seconds, the pump began to vibrate violently and make "popping" sounds from cavitating.

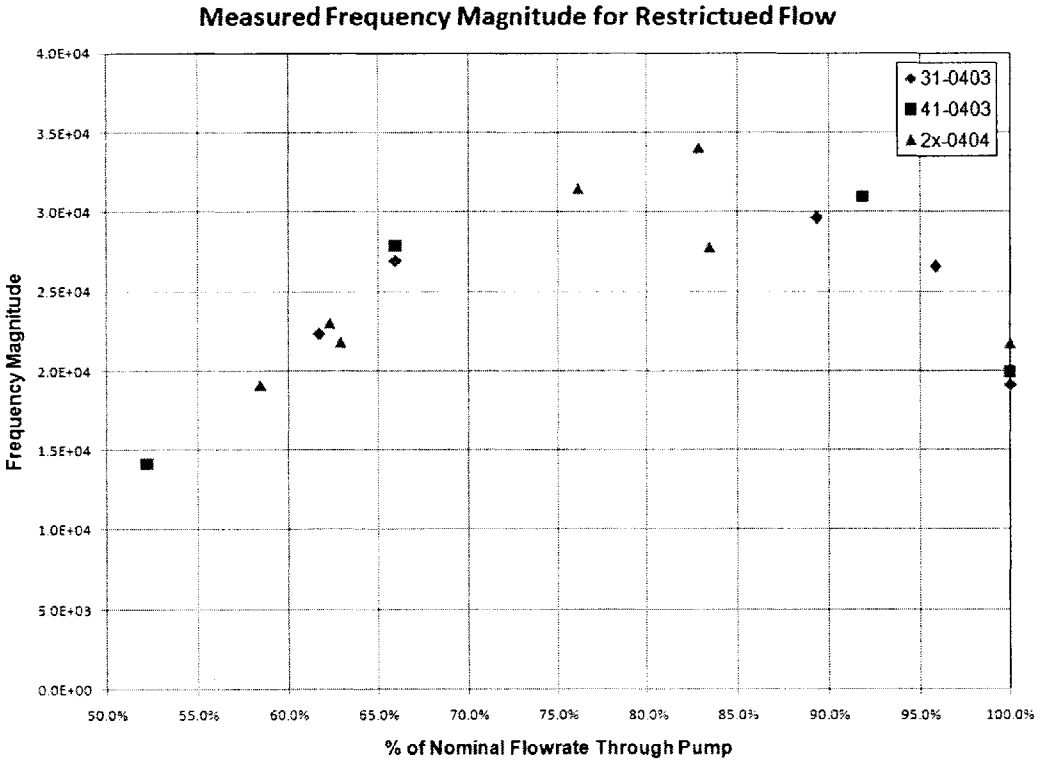

Figure 3-11: Test Stand Pump Motor Frequency Magnitude while Throttling the Inlet Valve

Figure 3-11 compares the pump power spectral content magnitude at 16 Hz to the pump flow rate. Pump cavitation was most apparent between 75% and 85% of the nominal pump flow rate. This region is also extremely sensitive to small inlet valve changes as indicated by the scatter of the few data points obtained in this region. The pump became air-bound below 65% of the nominal flow rate. This makes sense, as the impeded flow would make it difficult for the pump impeller to remain submerged. As prolonged exposure to cavitating conditions will reduce a pump's capacity, eventually destroying it, the NILM provides an inexpensive tool for monitoring systems at risk.

Another abnormal condition captured by the RO NILM is illustrated in Figure 3-12. Although the modulation is not as prevalent as in Figure 3-7 it is certainly detectable. Again looking at the spectral content it is clear that the 8.26 Hz magnitude ranging from 2.75×10^4 to 14.5×10^4 is driving the amplitude modulation. As it will be discussed in the following sections, this particular frequency has telltale properties that pertain to the HP pump. Although the cause of the modulation was never isolated, it is very similar the LP pump cavitation discussed earlier.

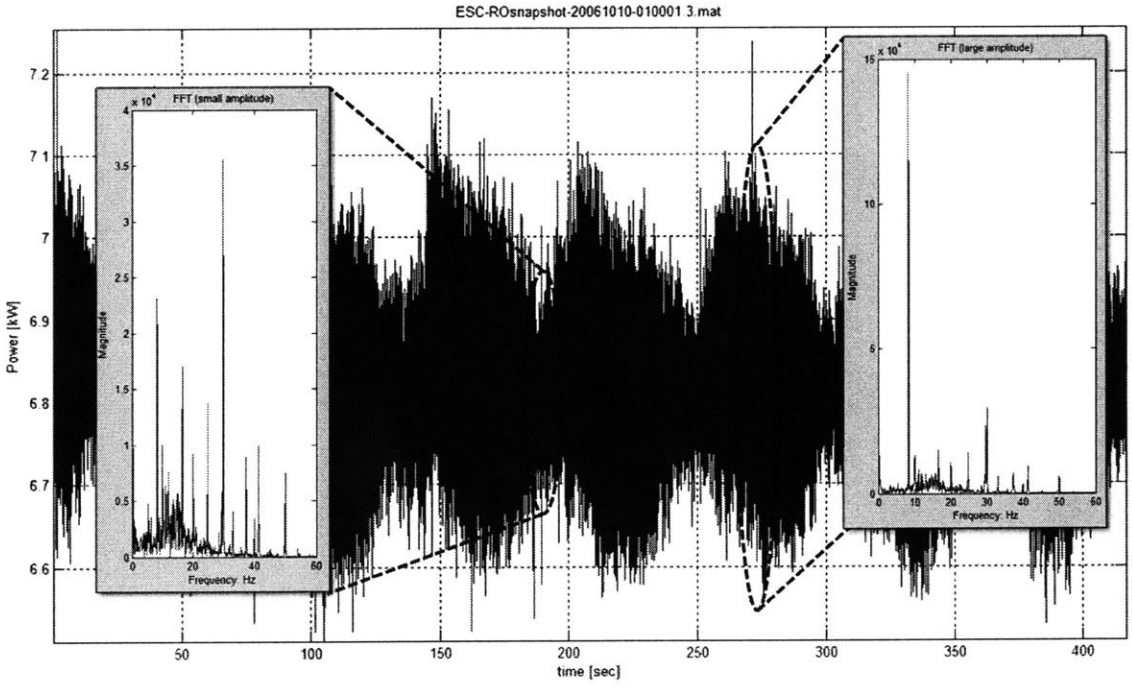

Figure 3-12: Abnormal HP Pump Power Modulation

3.2.1.3 *Pump Power Oscillations*

The large pump power oscillation shown in Figure 3-13 illustrates another abnormal condition recorded by the NILM. This trace was observed during the start immediately following the multiple restart behavior shown in Figure 3-6. When the HP pump came online, a large oscillation was observed. This oscillation, which has a remarkably large amplitude, continued for several days before it finally ended. The ship's crew had nothing to report when asked about the presence of any unusual noises or vibrations from the RO unit.

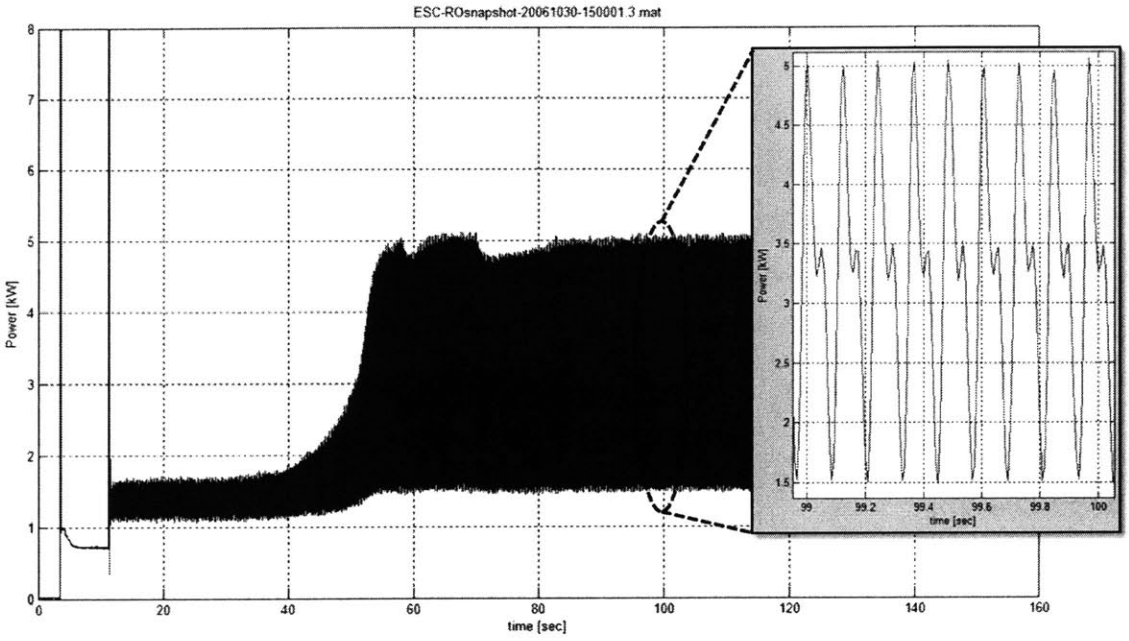

Figure 3-13: HP Pump Power Extreme Amplitude

The peak-to-peak time of the extreme amplitude wave shown in Figure 3-13 indicates a frequency of 8.26 Hz, which corresponds to the 495.7 RPM, measured from the HP pump shaft. This frequency can be isolated to the HP pump since the shaft is rotated by 1800-RPM motor through a 3.60:1 ratio v-belt drive as shown in Figure 3-14. The presence of this oscillation is clearly not healthy for the HP pump and requires immediate attention by the watchstander.

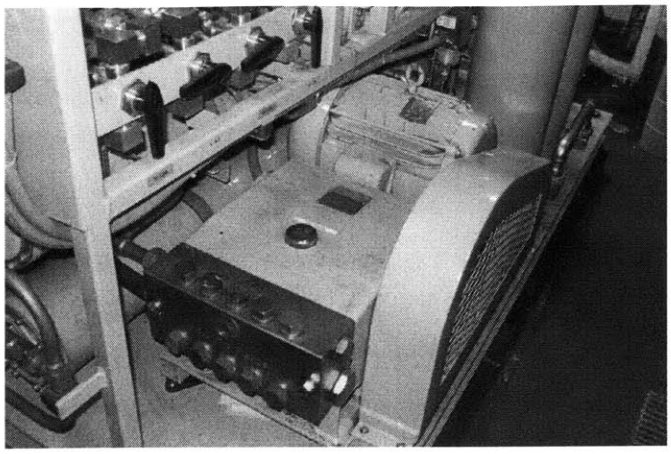

Figure 3-14: RO HP Pump and Motor with 3.6:1 Ratio V-belt Drive

It would be difficult to develop a diagnostics for every condition experienced by a fluid pump or the RO system, but by using the NILM to find abnormal power traces the operator can use this information to troubleshoot internal system problems not easily detected through conventional methods.

3.2.2 Condition Based Maintenance

Since the NILM monitors the power demand of a system in real-time with no interruptions, it becomes the ideal platform for trending component power demands. As trend analysis is one of the major pillars for a successful condition based maintenance program the NILM lends itself as a key tool for minimizing maintenance costs and unexpected equipment failures. The followings observations cover condition based maintenance indicators that have been resolved over the last year.

Figure 3-15 shows the frequency spectrum of the real power waveform presented in Figure 3-13. Note that there is significant spectral content at approximately 8.26 Hz and its harmonics. Later analysis found that there is always some significant amount of spectral content at this frequency, although its amplitude is not always so large.

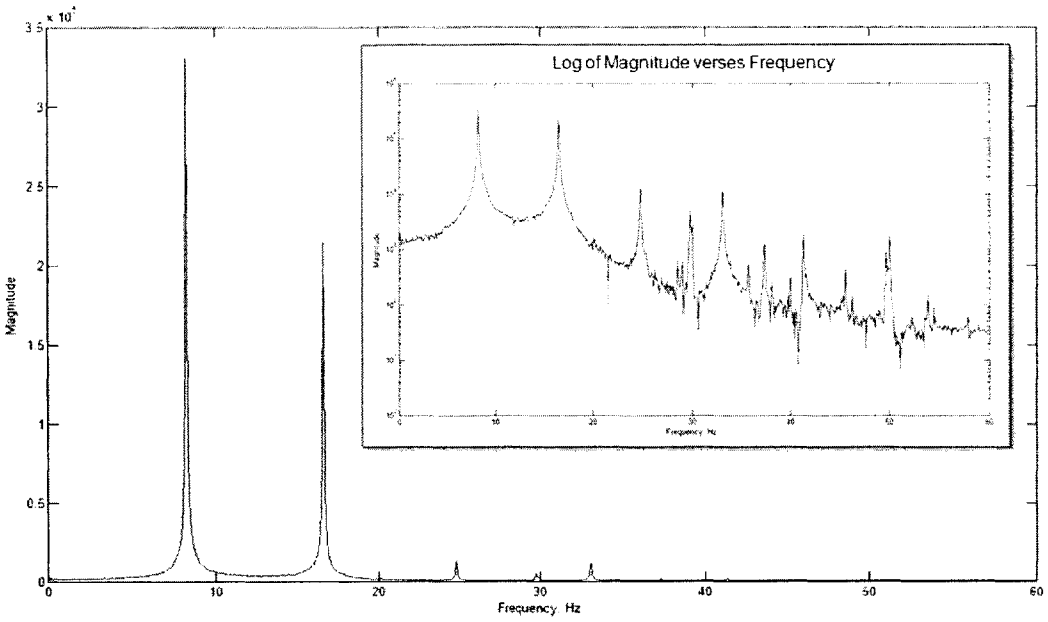

Figure 3-15: Frequency Spectrum Analysis of Figure 3-13

In fact, looking at a sample from each hour of the RO unit's operation indicates that the spectral content at 8.26 Hz is, for the short term, relatively consistent. As shown in Figure 3-16, the magnitude at this frequency for the *Escanaba*'s RO unit during February 2007 has a standard deviation of only 9.2%.

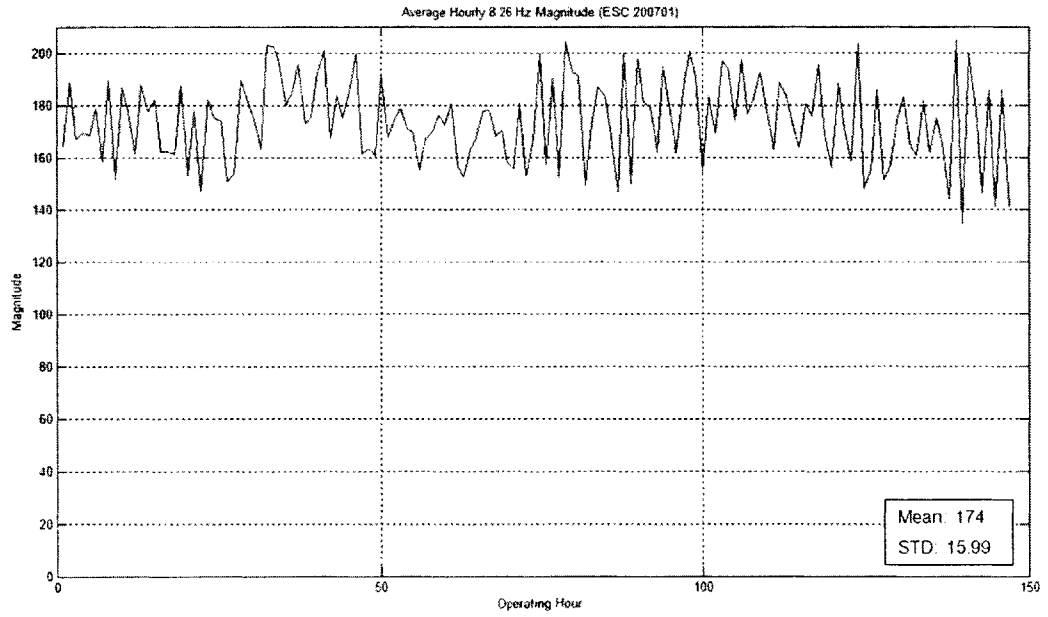

Figure 3-16: 8.26 Hz Hourly Trend for RO Unit Hp Pumps

Approximately two months after the discovery of the large HP pump power oscillation shown in Figure 3-13, the pump in question failed. As a preliminary test, the amplitude of the 8.26 Hz spectral peak was trended for over the past year. Figure 3-17 shows how the magnitude of this peak varied on several selected days between September 30, 2006 and February 1, 2007. The extremely high value recorded on October 30 corresponds to the behavior shown in Figure 3-13. It is interesting to note that the pump was replaced on December 21 following the discovery of damage to both the piston and the cylinder housing. Such a costly replacement could potentially have been prevented if the magnitude of the 8.26 Hz spectral peak had been trended in real time.

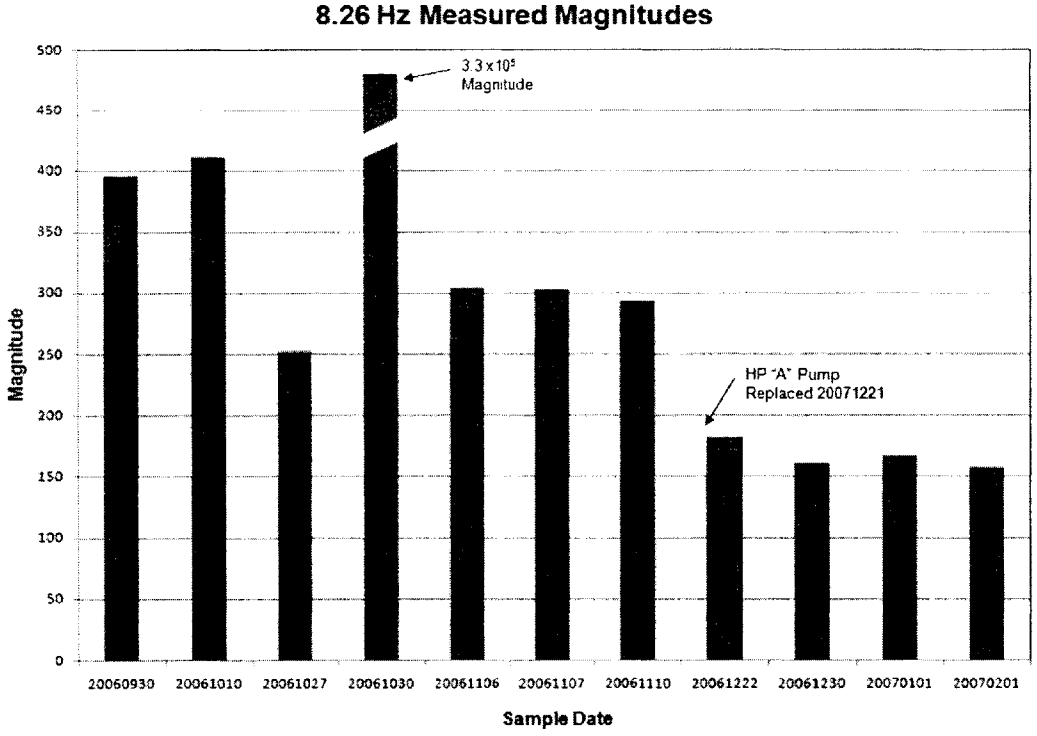

Figure 3-17: 8.26 Hz Magnitude Trending for RO Unit HP Pumps

The spectral content at 8.26 Hz is also dominant in the *Seneca*'s RO unit power demand. Additionally, they experienced an HP pump failure in June 2006 in which the pump had lost oil pressure and overheated, requiring complete replacement. Analysis of the before and after data for the *Seneca* reveals a 502% drop in the 8.26 Hz magnitude after the pump was replace. Given the availability of the spectral content at 8.26 Hz it is clear that a condition based maintenance routine could be conducted using the NILM for trend analysis.

3.3 Failure Detection

A sudden, unexplained, drop in system power demand is often one of the most easily detected and reliable indicators of a major component failure. For example, a pump-motor coupling failure would result in an immediate drop of motor power due to the sudden unloading. The same principle applies to the RO membranes. Unfortunately, without the NILM, the only indication of a membrane failure is a product water high-salinity alarm and the tripping of the solenoid dump valve (valve number V10 "A/B"). The high-salinity alarm is a generic alarm that can sound for any number of events and does not aid in troubleshooting the alarm origin. With the installation of a NILM, the operator has a second sensor that provides correlated power demand data for system components aiding in the isolation of a generic alarm.

Figure 3-18 depicts a 23% drop in the RO unit power demand due to a membrane failure onboard the *Seneca*. It took the crew nearly two days to isolate the cause of the high-salinity alarm and replace the membrane. During that time, the RO Unit was reduced to 50% capacity and no redundancy.

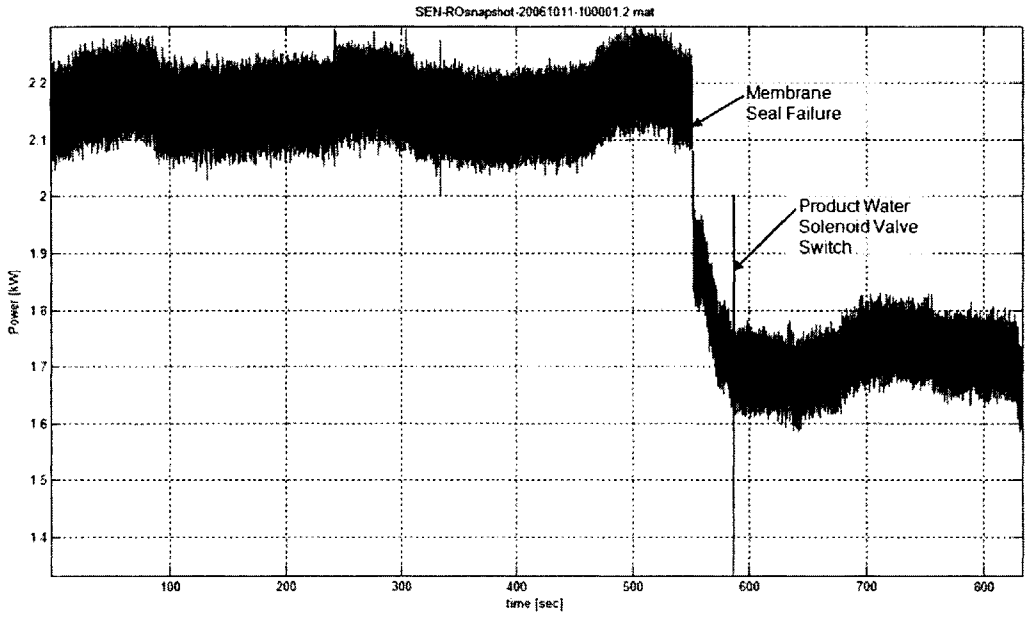

Figure 3-18: *Seneca* RO Unit Membrane Seal Failure Detection

Three semi-permeable membranes have failed in the past year between the *Escanaba* and *Seneca*. The frequency of this type of failure and time required to detect and repair the membrane make a strong argument for the NILM diagnostic capabilities. A simple algorithm

that monitors for a sudden system power drop while the pumps are still running would prove useful in detecting any number of major failures.

Another failure observed several times on both ships are the RO unit's HP pumps running while the system was in *standby*. The crews commonly refer to this scenario as a phantom start. The problem is so rampant that the watchstanders often open the circuit breaker to the RO unit after securing it from the master control consol to ensure no power reaches the pump motors. This type of failure significantly damages the positive displacement pumps as they are running dry and hot. With the LP pump secured the feed water is not being supplied to the HP pumps increasing the friction between the cylinder wall and plungers. Prolonged exposure to this condition drastically shortens component life and increases the chance of a catastrophic failure, where the ceramic plungers will disintegrate during normal operation. The phantom start malfunction is further accented by the failure of the inlet low-pressure switch interlock to prevent the HP pump running without sufficient feed water supply.

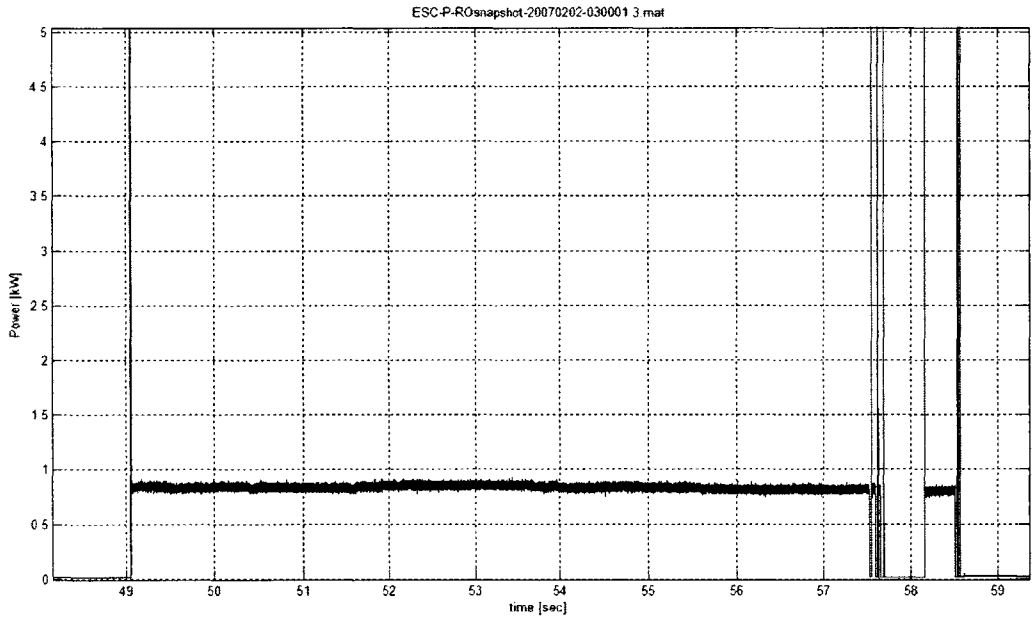

Figure 3-19: HP Pump running without LP Pump due to Master Control Consol Failure

Figure 3-19 provides an example HP pump phantom start where the RO unit was in *standby*. Note that the LP pump is not running during this time. The restart power spikes between 57.5 and 58.5 seconds are the result of the watchstander attempting to stop the HP pump from the

master control consul before securing power to the RO unit from the circuit breaker. By using the start sequence baseline discussed in Section 3.1, the NILM could diagnose an incorrect start and immediately alert the crew. Several instances have found the HP pumps running dry for over an hour before the crew detected the problem and secured the motor.

4 Filter Condition Modeling

Contamination can have a catastrophic effect on the positive-displacement pumps in an RO system. The following sections review the development and application of a filter condition model.

4.1 Filter Condition Influence on System Operation

Most contaminants are removed from the RO units onboard the USCG Cutters by the actions of the cyclone separators and the micron filters. As shown in Figure 2-6 and Appendix A, the separators pass a certain amount of fluid overboard. This ejected water contains most of the suspended solids found in the incoming feedwater with a specific gravity greater than 2.7; the subsequent micron filters remove any remaining particulates with diameters greater than 5μm. Over time, the filters become fouled with debris, resulting in an increase in the pressure loss, or differential pressure, across the filters and a decrease in the absolute pressure at the inlet of the positive-displacement pump. Because the loss in inlet pressure can result in harmful cavitation, the filters must be routinely cleaned or replaced. To assess filter status, watchstanders check the differential pressure across the filters each hour. To avoid human errors, relieve watchstander burden, and prevent sudden failures in highly contaminated waters, it is desirable to assess filter status using automated procedures.

One way to detect filter clogging in real time is to examine electrical power data. Robust, model-based detection methods can be developed by considering the inter-domain interactions that occur during a system start. As discussed in Section 3.1, the centrifugal (LP) pump is the first component to be energized. During the period when that pump runs by itself, it is solely responsible for pushing fluid through the micron filters and the overboard discharge. Thus, as the filter volume fills with water, the state of the filter will have a strong influence on the pump flow rate, which in turn will affect the current drawn by the pump motor. Because the positive-displacement pumps will impose a relatively constant flow rate once they reach a steady speed, [18], the filters have little effect on the flow once the HP pumps begin to operate. Thus, during the initial charging period, there is a unique opportunity to probe the effects of a change in the state of the micron filters.

4.2 Model Formulation

A relatively simple model can be formulated to describe the salient features of the pump-fluid interactions that occur during the initial filter-charging phase. Essentially, the centrifugal pump is creating the pressure difference necessary to move fluid through the cyclone separators and the micron filters. To a reasonable approximation, this means that the pump is driving fluid through a long pipe that eventually splits, providing some water to the filters and some to the overboard discharge path. In both the piping that follows the pump and the piping that carries discharged water overboard, one can approximate the head loss, $h(t)$, using the relation:

$$h(t) = \frac{l}{g \cdot A}\frac{dQ}{dt} + f(Q) \tag{4.2-1}$$

Where: $h(t)$ = head loss
$Q(t)$ = volumetric flow rate
g = gravitational constant
l = length of the pipe
A = pipe cross-sectional area
$f(Q)$ = energy loss due to the resistance of the pipe

This relationship, which considers only bulk fluid motion in the axial direction, is a simplification that accounts for inertial effects and energy loss [19] [20] [21] [17]. The loss term in Equation 4.2-1 is typically approximated using the D'Arcy-Weisbach formula, which states that:

$$f(Q) = kQ^2 \tag{4.2-2}$$

Where k is a constant that depends on both the geometry and properties of the pipe as well as the properties of the flowing fluid [19] [20] [17] [22].

During an initial start, the filter housing slowly fills wither water. As the volume fills, the amount of stored head increases. Assuming that there is a linear relationship between head and volume, the constitutive relation for this device is:

$$h = CV \tag{4.2-3}$$

Where: V = amount of water stored in the filter housing
C = filter element capacitance constant

In direct analogy with electrical systems, this device can be viewed as a capacitor. Although this model simplifies the actual physics, it does capture the relevant characteristics of the filter and it is often used in similar models [22]. The filter element capacitance constant, C, is a function of the filter element condition. In general, a clean filter would have a lower value for C than a fouled one. Assuming that C does not vary as a function of time, the flow rate through the device can be determined using the following relationship:

$$\frac{dh}{dt} = C\frac{dV}{dt} = CQ \tag{4.2-4}$$

The above arguments can be used to produce an overall model for the fluid subsystem. The model contains three states: the pump discharge capacity (Q_{IN}), the flow rate in the overboard discharge piping (Q_{DIS}), and the head across the filters (h_{OUT}). Neglecting any head loss in the piping ahead of the filters, it can be assumed that the filters and the discharge piping form two parallel paths with the same overall head loss, h_{OUT}. Assuming that compressibility is negligible, the continuity equation shows that:

$$Q_{IN}(t) = Q_{DIS}(t) + Q_{FIL}(t) \tag{4.2-5}$$

Where: Q_{IN} = pump flow rate capacity
Q_{DIS} = flow rate in the overboard discharge piping
Q_{FIL} = flow rate through the micron filters

The three state equations in the model are the following:

$$h_{IN}(t) = \alpha_{IN}\frac{dQ_{IN}}{dt} + k_{IN}Q_{IN}^2 \tag{4.2-6a}$$

$$h_{OUT}(t) = \alpha_{DIS}\frac{dQ_{DIS}}{dt} + k_{DIS}Q_{DIS}^2 \tag{4.2-6b}$$

$$C\frac{dh_{OUT}}{dt} = Q_{FIL}(t) = Q_{IN}(t) - Q_{DIS}(t) \tag{4.2-6c}$$

Where: α & k = represent system specific constants
h_{OUT} = head loss

In this model, Equation 4.2-6a describes the bulk motion of the fluid that is expelled by the pump, Equation 4.2-6b describes the bulk motion of the fluid in the discharge piping and Equation 4.2-6c models the flow through the micron filters.

The remainder of the overall model must account for the mechanics of the centrifugal pump and the dynamics of the motor that drives it. Such pumps produce an output head that exhibits a nonlinear dependence on both speed and flow. The salient characteristics of this dependence are captured using the relationship [19] [20] [23]:

$$h_{IN}(t) = a_1\omega_r^2 + a_2\omega_r Q_{IN} + a_3 Q_{IN}^2 \tag{4.2-7}$$

Where: ω_r = pump mechanical speed
$a_{1,2,\&3}$ = set of empirical constants

Similarly, the torque required to produce the head defined in Equation 4.2-7 can be specified as [19] [20] [23]:

$$\tau_m(t) = b_1\omega_r Q_{IN} + b_2 Q_{IN}^2 \tag{4.2-8}$$

Where: τ_m = motor shaft torque
$b_{1\,\&\,2}$ = another set of empirical constants

For a given speed, it is clear that Equation 4.2-7 and Equation 4.2-8 produce curves that are similar to those found in most manufacturer data sheets. Including viscous friction, the net torque becomes:

$$J\frac{\partial\omega_r}{\partial t} = \tau_e - \tau_m - \beta\omega_r \tag{4.2-9}$$

Where: J = moment of inertia
τ_e = torque of electromechanical origin
β = coefficient of viscous friction

The complete simulation model must include the electrical state equations for the three-phase induction machine. In the synchronously rotating d-q reference frame, these equations are [24]:

$$\frac{\partial \lambda_{ds}}{\partial t} = v_{ds} + \omega\lambda_{ds} - r_s i_{ds} \tag{4.2-10a}$$

$$\frac{\partial \lambda_{qs}}{\partial t} = v_{qs} - \omega\lambda_{ds} - r_s i_{qs} \tag{4.2-10b}$$

$$\frac{\partial \lambda_{dr}}{\partial t} = v_{dr} + (\omega - p\omega_r)\lambda_{qr} - r_r i_{dr} \tag{4.2-10c}$$

$$\frac{\partial \lambda_{qr}}{\partial t} = v_{qr} - (\omega - p\omega_r)\lambda_{dr} - r_r i_{qr} \tag{4.2-10d}$$

Where:
- λ_{ds} = direct-axis stator flux
- λ_{qs} = quadrature-axis stator flux
- λ_{dr} = direct-axis rotor flux
- λ_{qr} = quadrature-axis rotor flux
- r_s = stator resistance
- r_r = rotor resistance
- i_{ds} = direct-axis stator current
- i_{qs} = quadrature-axis stator current
- i_{dr} = direct-axis rotor current
- i_{qr} = quadrature-axis rotor current
- v_{ds} = direct-axis stator voltage
- v_{qs} = quadrature-axis stator voltage
- v_{dr} = direct-axis rotor voltage
- v_{qr} = quadrature-axis rotor voltage
- p = number of pole pairs
- ω = frame speed
- ω_r = rotor mechanical speed
- ω_p = pump mechanical speed

The overall eighth-order model consists of Equations 4.2-6a/b/c and Equations 4.2-10a/b/c/d. Examining the equations it is expected that the pump motor will take longer to reach a steady-state condition given a clogged filter. The steady-state condition is defined as the time the pump motor power demand gradient goes to zero for the long term. The steady-state condition *does not* occur at a local minima or maxima. Equation 4.2-11 expresses this sate as a derivative of the pump motor power demand.

$$\frac{\partial P_m(t)}{\partial t} = 0 \qquad (4.2\text{-}11)$$

Where: $P_m(t)$ = pump motor power with respect to time

As shown by the model, the measured time the pump motor takes to reach the steady-state condition is relative to the value of C and is an assessment of the filter element condition. This measurement is referred to as the steady-state start transient time.

4.3 Model Results

MATLAB® was used to encode the pump start transient model for simulations with various filter conditions. The data CD referenced in Appendix D provides the pump-filter simulation script files. The filter condition was set by changing the value of the filter element capacitance constant, *C*, from Equation 4.2-6c. A larger *C* indicates an increase in the filter clogging condition.

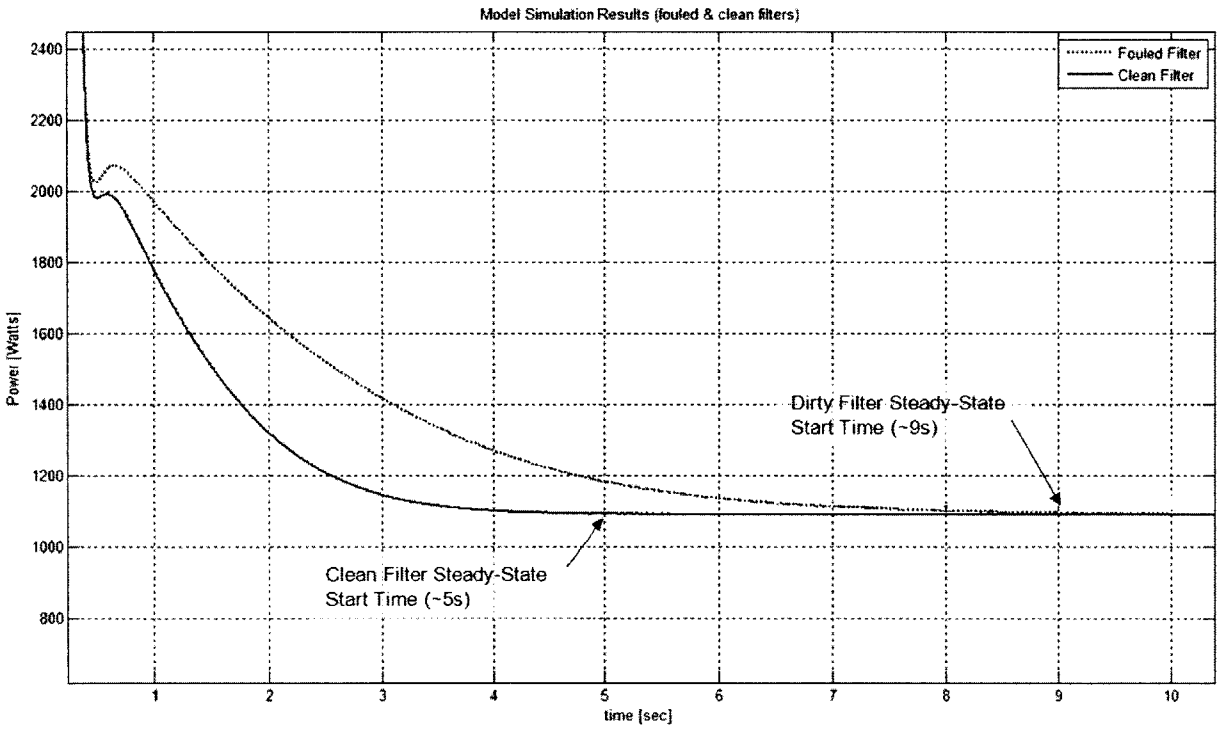

Figure 4-1: Pump Motor Real Power from Filter Condition Model

The results from the filter condition model simulation, shown in Figure 4-1, support the premise that the steady-state start transient time is smaller for the *clean* filter condition. In this case, there was a difference of approximately 4 seconds between the *clean* and *fouled* filter conditions. Comparing the pump volumetric flow rate in Figure 4-2 to the *fouled* filter pump motor power demand in Figure 4-1 demonstrates the relationship between the two parameters as indicated by the similarity between their gradients. It is also interesting to note that both parameters have a steady-state start transient time of approximately 9 seconds.

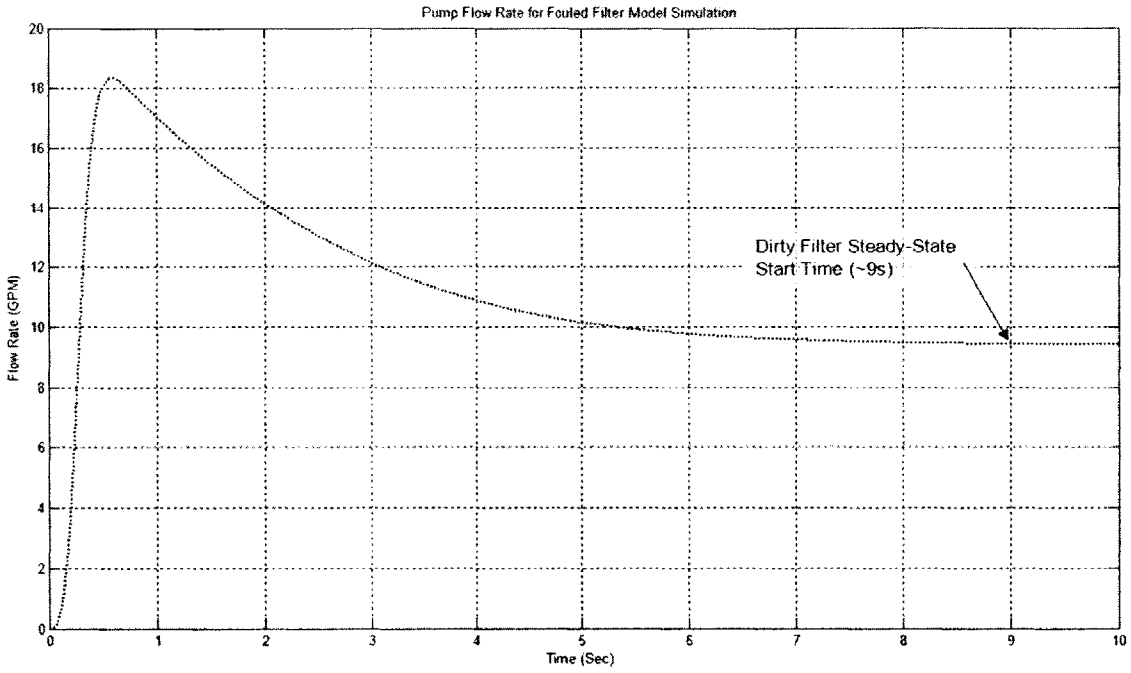

Figure 4-2: Pump Volumetric Flow Rate for Fouled Filter Condition Model

The filter condition model simulation clearly demonstrates the dependence between the pump flow rate and power demand. This reliance can be used as a reliable way to determine the filter condition based solely on the pump motor steady-state start transient time without the need for additional sensors. In summary, the time at which the pump power demand gradient goes to zero is directly relative to the condition of a down-stream filter.

5 Filter Condition Diagnostics

5.1 Pump Motor Steady-State Start Time

The theory and model discussed in Chapter 4 indicates that the pump motor steady-state start transient time is relative to the downstream filter condition. With this in mind, several conditions must exist for independent pump start evaluation:

- For the steady-state start transient time to be comparable with other starts, the fluid system must start from a consistent state. This means that fluid levels throughout the system, including the filter housing, drain down to the same prestart condition before the next pump start occurs. This condition stipulates that the pump transfers the same volume of fluid to charge the system for each start.
- The steady-state start time is only valid for the initial pump motor start. If several pump starts are initiated in quick succession, the first condition fails, as the empty system volume is different for each start. This will adversely influence the steady-state start time. If the system is allowed to settle to its normal prestart state then following start is valid for measurement.
- A consistent pump start procedure is used for each start. This means the system valve alignment and sequence of events is the same for each steady-state start time analyzed.

5.2 Trend Analysis

Progressively tracking the steady-state start time for each pump start will provide a trend of the filter condition. As each filter and pump system is different, the absolute cut-off steady-state start time, where the filter needs to be cleaned or replaced, will vary. Baseline measurements can be used for a clean and fouled filter condition to assess the steady-state start transient times indicative of a particular system configuration. Using trend analysis allows the operator to observe changes in the systems performance over time and to evaluate each start based on the requirements outlined in Section 5.1.

5.3 Laboratory Experiments

Several sets of experiments were conducted to investigate filter condition indicators present in the pump power start transient and confirm the model developed in Chapter 4 applicability. The intent of these experiments was to model the reverse osmosis (RO) unit startup sequence between the LP pump start and before the HP pump start and determine if there were any reliable filter condition indicators present in the LP pump start transient power.

5.3.1 System Setup and Procedure

The laboratory test stand was modified to simulate the start sequence of the RO unit by capping the discharge pipe from the filter housing. This setup models the blocked-flow effect caused by the secured HP pump before it is started. A 0.10-inch diameter hole was drilled in the cap to vent air as the filter housing was charging; this is similar to the "air/oil bleed" located at the top of the RO unit's micron filter housing [14]. To simulate the constant discharge flow from the RO unit's cyclone separators, valve-1 on the test stand was partially open with 2 turns while valve-2 was completely closed. Valve-3, which leads to the filter housing, was completely open for the experiments. The valve locations and nomenclature are identified in Figure 2-9.

Clogging was simulated by wrapping the filter element, shown in Figure 2-10, with paper towels held in place using fiberglass window screen material and four rubber bands. A total of two paper towel wraps and six screen wraps were used to represent a fouled filter. Initial testing showed that complete coverage of the filter element by the fouling material is required to induce the full clogging effect. Since the clean filter element is very porous, it has little influence on the differential pressure across the filter housing. Any area of the element not covered by fouling material will easily allow flow and skew the results.

To ensure that the empty volume of the filter housing was consistent for each start, the filter housing was completely drained between each test run. Additionally, the greater volume of the fouled filter was accounted for by adding 380 mL of water to the filter housing before the clean filter starts. Table 5-1 provides a list of the measured volumes for the filter housing, clean filter element, and fouled filter element.

Table 5-1: Test Stand Filter Component Volumes

Component	Volume
Filter Housing Volume	3200 mL
Clean Filter Volume	680 mL
Fouled Filter Volume	1060 mL

The experiment was divided into 13 runs. Each test run was initiated by starting the centrifugal pump motor. After running the motor for 12 seconds, it was stopped and the filter housing drained. If required, the filter condition was modified at this point. The start transients for four different system configurations were examined:

- Fouled Filter: with 2 paper towel and 6 screen wraps
- Clean Filter: with 380 mL of water added prior to the filter housing before the start
- No Filter: with the filter element removed and 1060 mL of water added before the start
- Filter Bypassed: with valve #3 closed to bypass the filter housing before the start

Data was collected using an eight channel NILM as specified in Section 2.4.2 and Table 2-6. Appendix C provides the MATLAB® scripts used to process, collate, and display the recorded data from the test stand.

5.3.2 Laboratory Test Stand Results

The test stand experiments support the filter condition model and conclusions discussed in Chapter 4. As shown in Figure 5-1, a noticeable difference exists between the pump motor real power demand for each filter condition. In particular, it is interesting, and expected, that when the filter housing was bypassed by closing valve-0 the pump motor immediately reached steady-state in 0.5 seconds without the characteristic "hump" present in the other two examples. This comparison clearly shows the effect of the filter housing being filled with fluid, or charging, has on the pump power demand. Also, note the 1-second lag in the steady-state time between the clean and fouled filters.

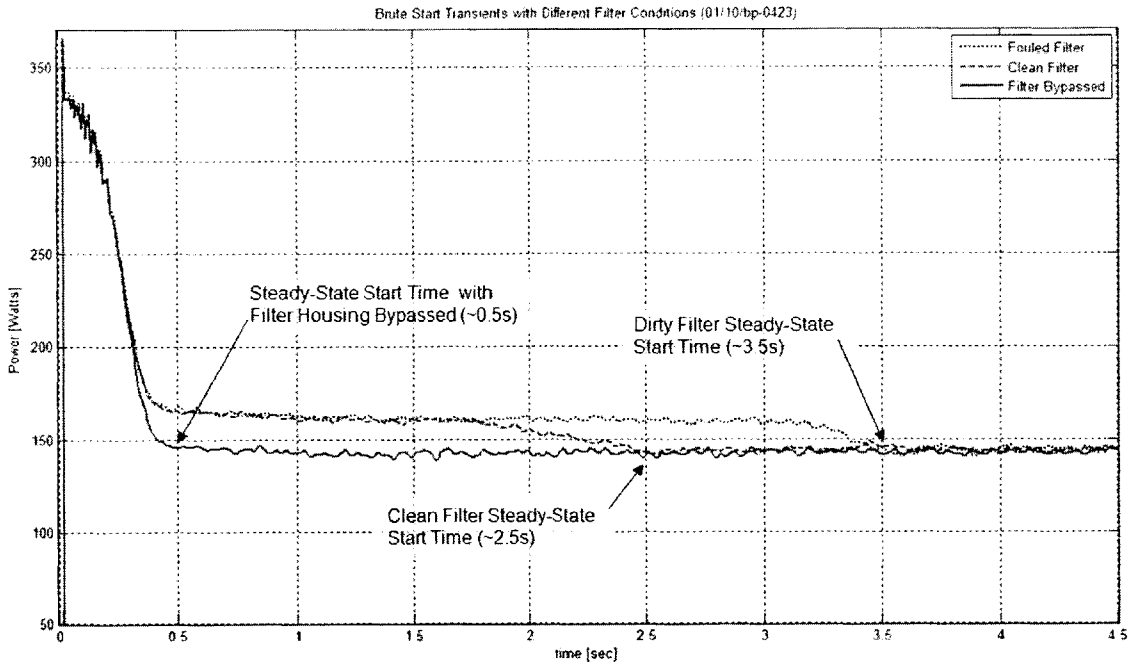

Figure 5-1: Laboratory Test Stand Pump Power Comparison for Various Filter Conditions

Figure 5-2: Laboratory Test Stand Pump Flow Rate Comparison for Various Filter Conditions

Comparing the measured flow rate in Figure 5-2 for the same three tested conditions in Figure 5-1 confirms the relationship between the pump power and its flow rate. As discussed in Chapter 4, when the slope of the real power traces goes to zero the flow rate also goes to zero marking the steady-state start transient time. Note that the flow rates reach a steady-state value of 40 GPM in each case. The small discrepancy in steady-state time for the flow rate is due to the discrete nature of converting the flowmeter pulse period to a frequency. The 0.1-second difference that exists between the real power and flowmeter steady-state time for the clean filter condition is certainly within the experiment's tolerances needed for validating the filter condition diagnostic. Although this was discussed extensively in Chapter 4, the test data confirms the applicability of the developed system model.

One particularly interesting feature in Figure 5-2 that is present for the fouled and clean filter flow rates is the noticeable dip in flow rate just after 1 second. This valley does not correspond to any real power trace features shown in Figure 5-1. The experiments were not setup to evaluate this particular characteristic, but one possibility is the slight change in flow characteristics as the fluid initially discharges into the reservoirs from the piping system connected by valve-1.

The complete, time synced, data sets from the clean and fouled filter conditions are available in Figure 5-3 and Figure 5-4. Many conclusions can be easily drawn about impact of the filter condition on the respective start transients by comparing the two figures. It is interesting that in both cases the filter housing charging time is clearly indicated by the small oscillation from the filter differential pressure sensor. Also, note that this sensor goes to zero, or its prestart level, shortly after the filter charging is complete. This is expected as the pressure on both sides of the filter housing has equalized by this time. The lag between the completion of the filter housing charging and the pump real power steady-state time is the due to the system response to the change in both flow rate and pump differential pressure. As the pressure of the filter housing equals the pump discharge pressure, minus pipe losses, flow to the branch disappears as shown by the gradual reduction flow rate through pump.

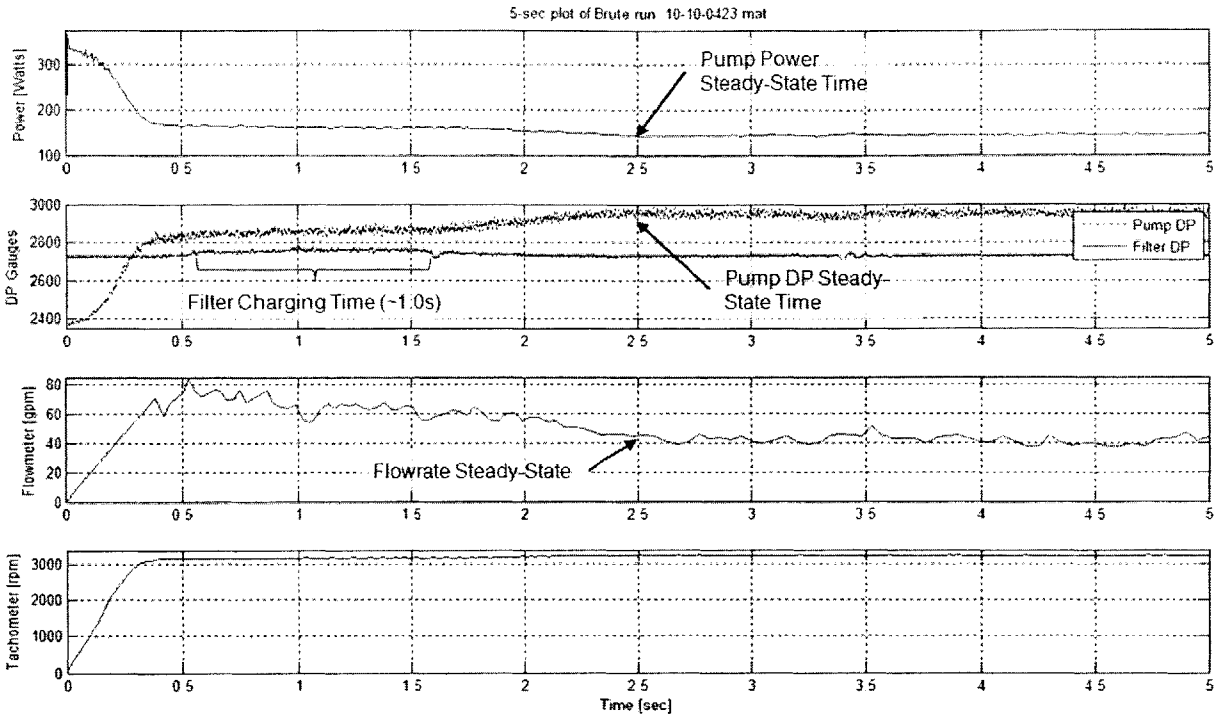

Figure 5-3: Complete Data Set for a Clean Filter Start on the Test Stand

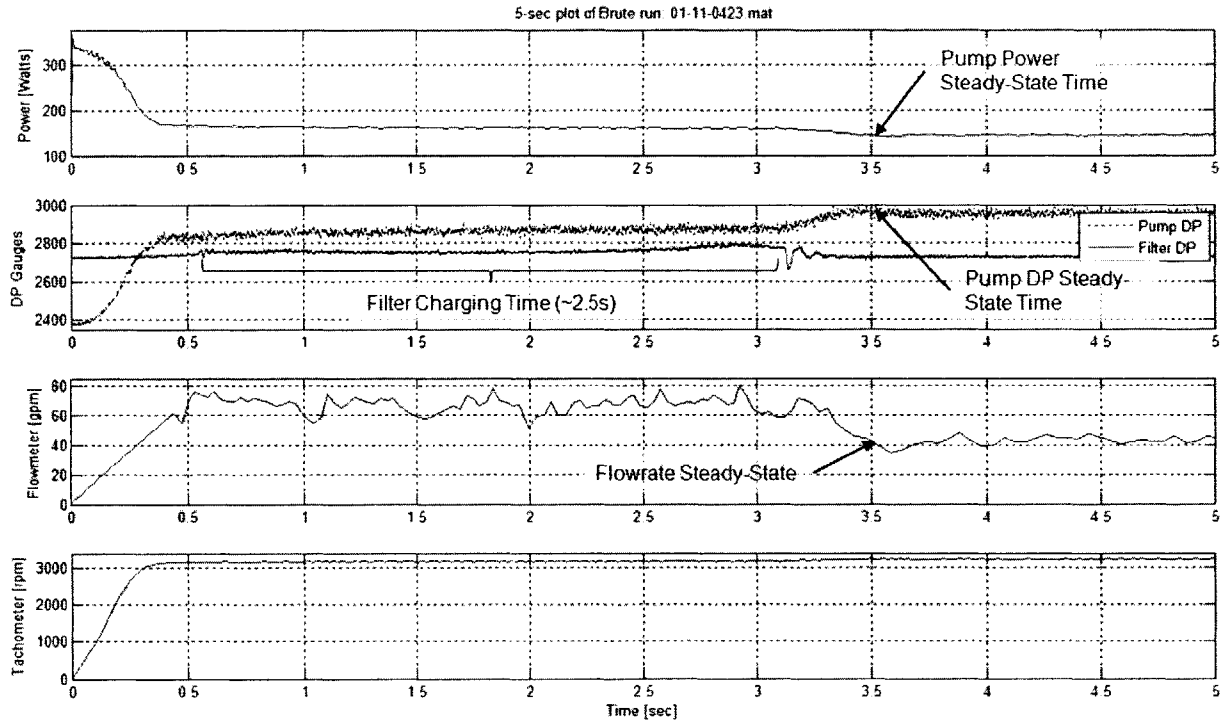

Figure 5-4: Complete Data Set for a Fouled Filter Start on the Test Stand

Although it is difficult to see in Figure 5-3 and Figure 5-4, pump rotational speed increases by approximately 20 RPM just as the pump motor power transitions to steady-state. This is expected as the pump motor experiencing a smaller load at this point then during the start transient as indicated by the flow rate, causing the pump motor to speed up. Although the flow rate is halved during this transition the pump differential pressure does go up mitigating some of the unloading effects.

A comparison of the pump motor real power and pump flow rate between the *clean* and the *no* filter conditions indicates very little difference between the two start transients as shown in Figure 5-5 and Figure 5-6. Since the measured differential pressure across the filter housing for the *clean* filter condition was within 5% of the *no* filter condition these figures validate the practice of adding fluid to the filter housing to maintain a consistent initial empty volume for each start.

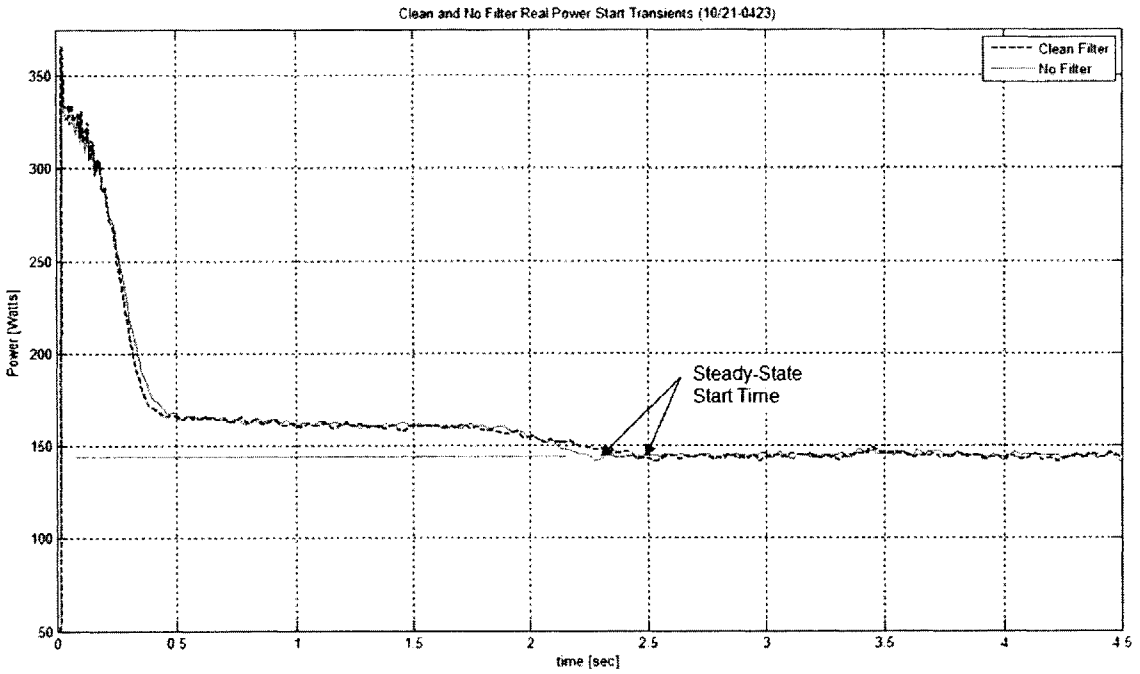

Figure 5-5: Pump Motor Real Power Comparison for *Clean* and *No* Filter Conditions

It is also interesting to note that the steady-state start time is 0.25 seconds longer for *clean* filter start as the measured differential pressure across the filter housing was slightly higher for this

condition. The comparisons shown in Figure 5-5 and Figure 5-6 provide an excellent example of how sensitive the pump motor power is to small filter condition differences. Finally, the dip in the flow rate initially identified in Figure 5-2 is also present for the *no* filter pump start just after 1 second of running time.

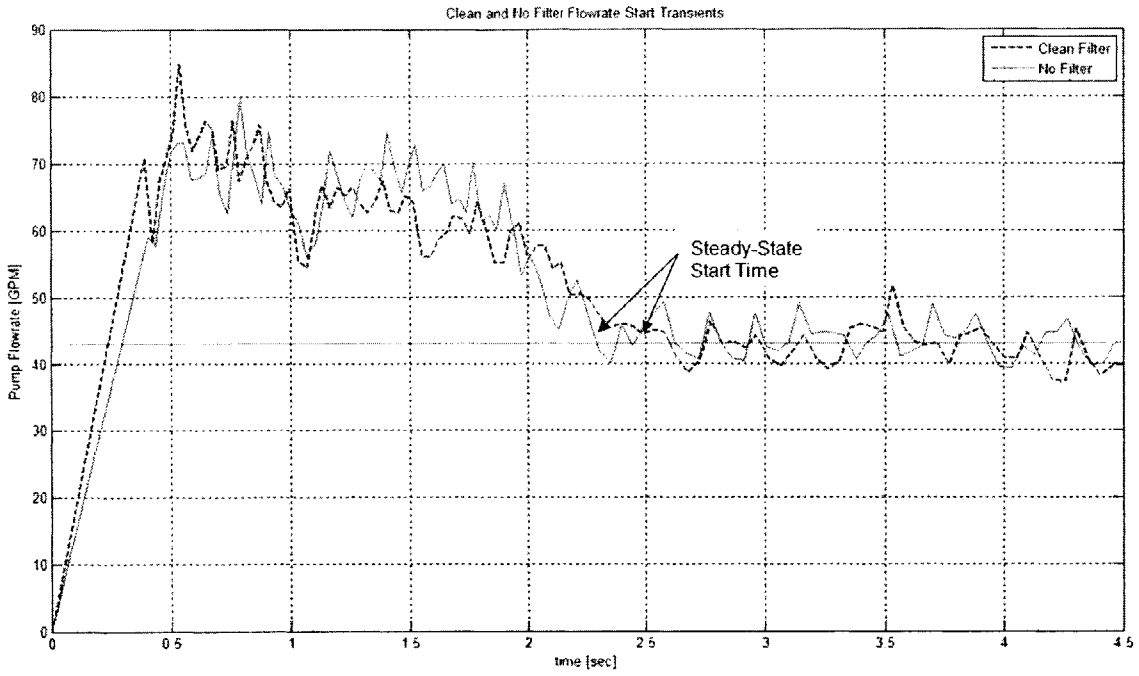

Figure 5-6: Pump Flow Rate Comparison for *Clean* and *No* Filter Conditions

The conclusive results attained from the laboratory test stand support the assumptions needed to create the filter condition diagnostic model. Additionally, these experiments provided an excellent starting point for analyzing the RO NILM data, where the only measured system property is the LP pump motor power demand.

5.4 Field Experiment

The primary intent of the field experiment was to verify the start transient characteristics measured from the laboratory test stand and to determine if the NILM unit could capture the pump power steady-state time on the RO units. The *Escanaba* was very helpful in providing personnel and allowing the experiments to be run while inport.

5.4.1 Experiment Setup and Procedure

The field experiment runs were conducted in accordance with RO unit start procedure outlined in the technical manual [14], also identified in Section 3.1.3. In general, the start procedure assumes an initial system alignment where both the LP and HP pumps are secured and both the raw water isolation valve (V2 "A/B") and the HP bypass valve (V6 "A/B") are opened. The operator then starts the LP pump manually from the master control consol and the HP pump is started after the inlet pressure has stabilized. The HP bypass valve (V6 "A/B") is finally closed increasing the membrane pressure between 800 and 1,000 psi. At this point, the product water was sent overboard using the *mode* selection on the master control consol. The RO unit was allowed to sit idle for 5 minutes between each run. This allowed the filter housings to drain to consistent state.

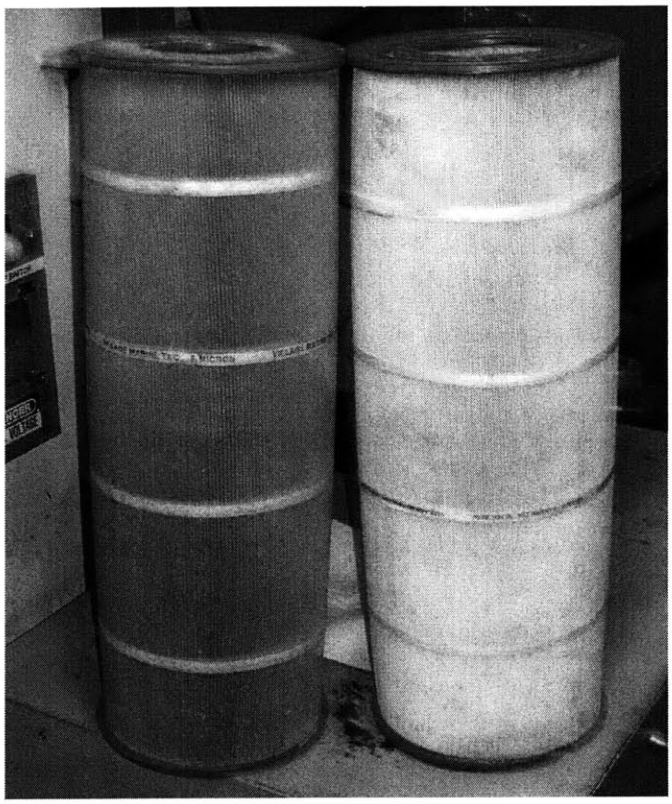

Figure 5-7: Filters used for *Escanaba* LP Pump Start Transient Experiment

The Escanaba graciously saved a set of fouled filter from their last underway. Figure 5-7 compares the fouled and clean filters used for the experiment. The measured filter differential

pressure for the fouled filter was 18 psi while the clean filter had a differential pressure of only 4 psi. The experiment included eight starts recorded by the NILM; four for each filter condition.

5.4.2 Field Experiment Results

Comparing the real power traces between the fouled filter and the clean filter starts it is clear that the steady-state start transient time increases with the filter differential pressure as found in the laboratory experiment. Figure 5-8 provides the aggregate real power start transient demand for a clean and dirty filter. The second power spike on the clean filter trace at 14 seconds is the HP pump starting. At approximately 26 seconds, the LP pump steady-state start time for the fouled filter condition is more than twice that of the clean filter's 12-second steady-state start time.

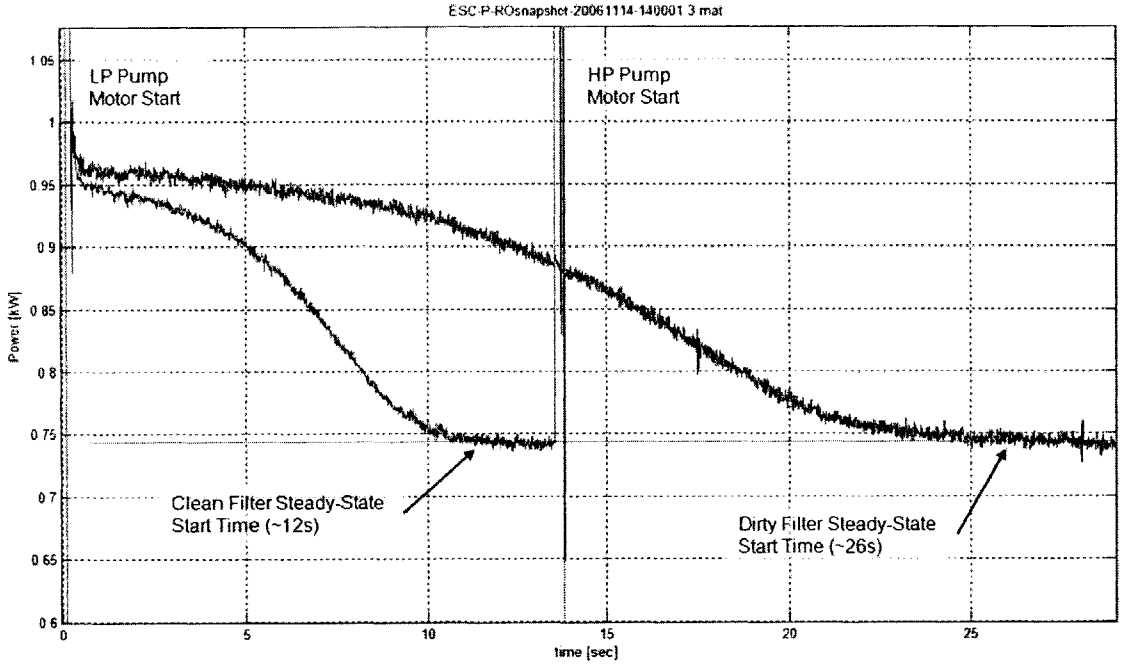

Figure 5-8: Real Power Traces for *Escanaba* LP Pump Start Transient Experiment

The field experiment results collaborated nicely with the model and laboratory experiment data, confirming the NILM's ability to monitor the LP pump start transient.

5.5 Underway Data

The final step to verify the practical application of the steady-state start time as a filter condition diagnostic tool was to sample and compare underway data to recorded micron filter differential pressure readings from the operating logs.

5.5.1 Data Collection

Underway data was collected continuously using the NILM configurations stated in Section 2.3.3. The *raw* data was uploaded from the PC to the laboratory server and run through *prep* for analysis. Initially, the 6-channel data collection on the Escanaba was hindered by PCI-1710 card problems. Due to the uninterrupted 48,000 Hz collection rate, the data for each hour did not completely transfer to the hard drive, only saving segments of each hour for analysis. The PCI-1710 card software was modified in November 2006 to correct the data transfer rate problem and the NILM was been working reliably since.

As this data was collected under a variety of operating conditions not every start was suitable for start transient analysis. In general, about 10 to 20 percent of the recorded RO unit starts are not in accordance with the procedure outlined in the manual [14] resulting in unusual power traces. In most cases, the valves were misaligned or the watchstander attempted to start the HP pump before the inlet pressure was sufficient to disengage the low-pressure interlock switch. Looking at the examples available in Chapter 3 it is clear that a simple parametric could be used to identify flawed RO unit starts.

Finally, as the ship was underway with a constantly varying position the data collected represents a dynamic environment of changing raw water temperatures, salinities, and particulate concentrations. These conditions provided a wide array of start situations for analysis and enabled the opportunity to measure the robustness of the proposed filter condition diagnostic indicator.

5.5.2 Analysis Methods

The first implementation of the steady-state start transient time diagnostic indicator was to use a visual comparison. Although a mathematical approach would provide more consistency within

the analysis the visual method was chosen to increase the number of suitable RO unit starts and to observe the range of possible start profiles. The visual comparison was conducted using a baseline start transient profile that was known to have a clean filter. The baseline was then compared to each suitable start to consistently identify where the real power slope goes to zero.

5.5.3 Underway Results

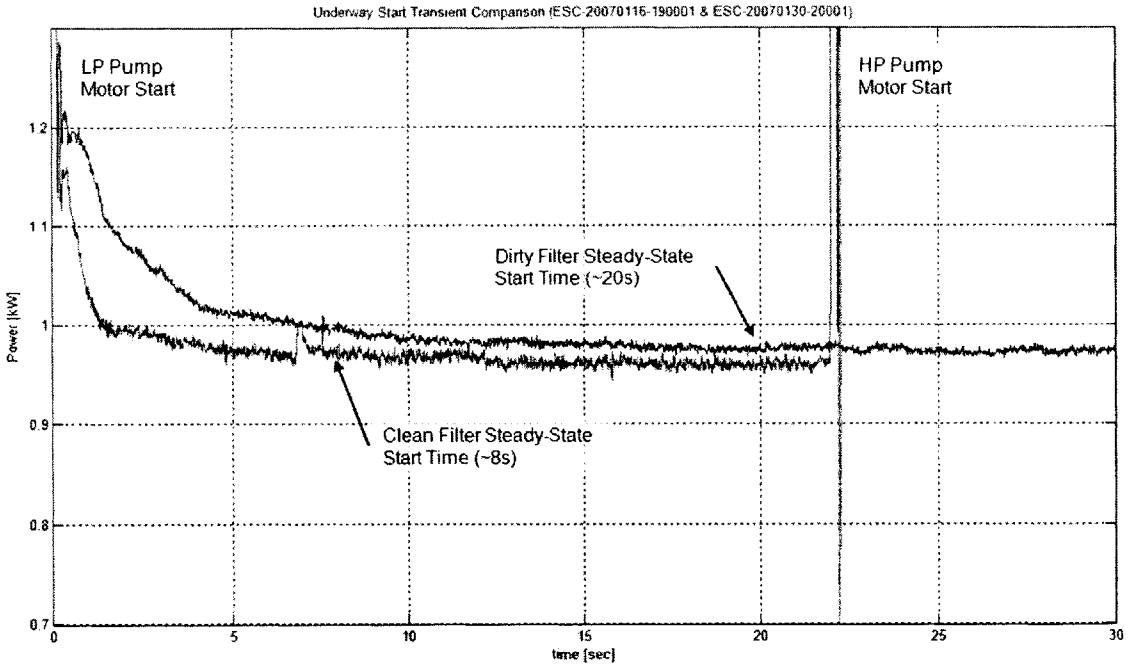

Figure 5-9: Sample of Collected *Escanaba* Underway Data

Although the underway LP pump start transients shown in Figure 5-9 were not as smooth as the experimental and laboratory data they matched the filter condition model gradient developed in Chapter 4 remarkably well. The difference between the steady-state power magnitudes is likely a combination of the extremely dynamic shipboard environment and the several day lag between starts. The samples shown are *Escanaba* LP pump start comparisons from *before* and *after* a micron filter replacement on 30 January 2007. It is important to note that although these start transients have different slope profiles than previously shown from the experimental data, the steady-state time can still be determined by ascertaining where the real power demand slope goes to zero. This exhibits the robustness of the steady-state start transient diagnostic algorithm.

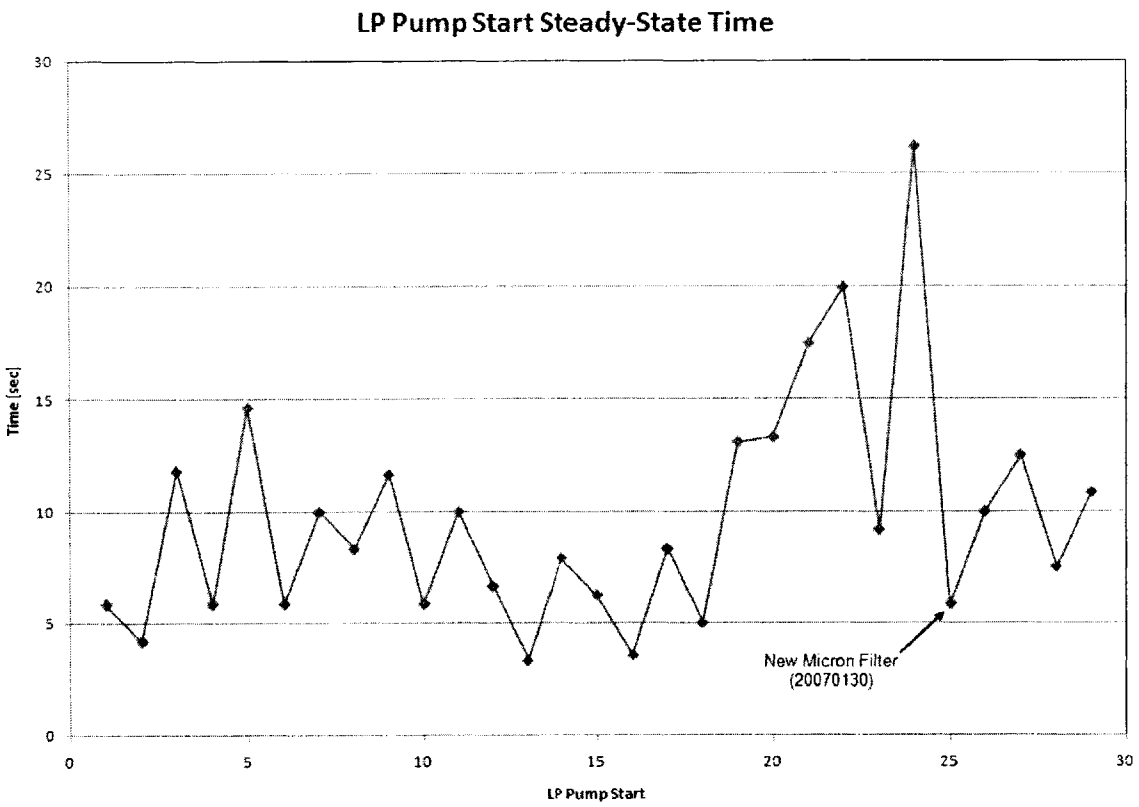

Figure 5-10: LP Pump Start Transient Steady-State Time Trend Analysis for January 2007

Figure 5-10 provides the LP pump start transient steady-state time trend analysis for January 2007 onboard the *Escanaba*. The apparent fluctuation between each steady-state start time is in line with micron filter differential pressure variation recorded in the RO unit logs. The differential pressure variation is the result of many factors such as non-uniform filter fouling and abrupt changes in feed water quality. Even with the fluctuating steady-state start time the data trend clearly indicates a drastic increase in time just before the filter is replaced due to the high differential pressure across the micron filter housing.

6 Cost Analysis for Monitoring Shipboard Fluid Systems

6.1 Motivation

Modern naval vessels are becoming increasing dependent on electricity for energy distribution. In the past, many shipboard systems functioned on steam or compressed air, but the trend is for greater reliance on electrical power with each new ship-class. This trend is illustrated in Figure 6-1 where the electric generating capacity of U.S. Navy Destroyers has consistently increased over the last century.

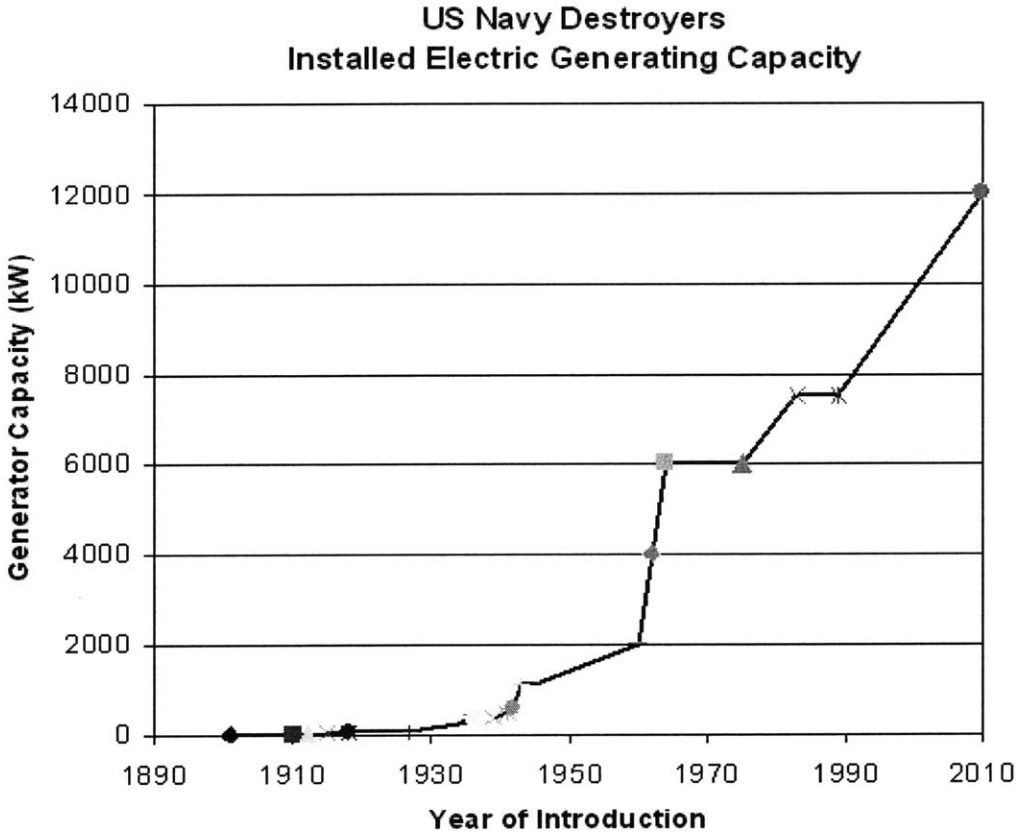

Figure 6-1: Electric Generating Capacity of U.S. Navy Destroyers (1910-2010 projected) [6]

Although concepts like the "all electric ship" and rail gun certainly add to the need for additional electric power generation capacity, they are not the only reason for continued increases. Systems that were originally steam driven have been replaced by the electrical equivalent during major ship availabilities. This process is an effort to increase the life of the ship while simplifying the

primary energy distribution system and improving overall energy conversion efficiency. One prime example of this process is the back-fit of the U.S. Coast Guard's Famous Class Medium Endurance Cutters from steam powered distilling plants to electric reverse osmosis units (RO) for water making. Although the back-fit eliminated the need for shipboard steam generation, it added a significantly more complex computer-driven water making system. The additional complexity of the RO unit, although more reliable, requires substantially more sensors and monitoring. In fact, the RC7000 RO unit has 18 sensors and monitors compared to the original distilling plant's 6 gauges and one sensor [14].

Increasing shipboard sensor and monitoring requirements is a contradiction to efforts for reducing ship's force personnel. Not only do the sensors require monitoring, they also have maintenance and calibration needs. The sum of monitoring, maintaining, and calibrating these sensors throughout the entire ship can account for a significant portion of crew man-hours. The GAO report titled, "Navy Actions Needed to Optimize Ship Crew Size and Reduce Total Ownership Costs", specifically details the need for human systems integration to effectively reduce shipboard personnel requirements [25]. Systems that require more monitoring and maintenance, unless properly integrated, could actually increase watchstanding needs and drain available man-hours. Balancing improved system energy conversion and distribution simplification with reduced manning clearly results in lower ship operating costs. NILM can aid with human integration elements while simplifying system-monitoring and reducing maintenance requirements.

6.2 Cost Considerations

6.2.1 Manning Costs

The U.S. Navy actual Military Personnel (MilPers) costs for FY06 was $37.8B accounting for 28.7% of the Department of the Navy's (DoN) $131.9B budget [26]. With the DoN's average active strength, including sailors and marines, at 364,684 the direct cost per sailor is $103,700 [27]. This does not include training and infrastructure support costs, which are included in the DoN's $40.6B Operational and Maintenance (O&M) costs. The U.S. Coast Guard (USCG) and DoN utilize the same pay scale and similar rating (job) structure, therefore individual sailor costs

are assumed to be similar. Looking at these numbers it becomes very clear that placing extra quality personnel onboard ships cost prohibitive.

During normal operations, the sound and security watch visits the auxiliary space where the RO unit is located to log gauge and sensor readings each hour. It takes approximately 2 minutes to read and record the 18 RO data outputs. A supervisor does not usually review these logs until the end of the four-hour watch or after a failure. In practice, the RO unit operates unmonitored 97% of the time, delaying the initiation of casualty control actions. In fact, given the nature of the watch, most RO unit failures go undetected for several rounds, as the first indications are not prevalent in the hourly readings. These circumstances were observed in four of the six failures analyzed from field data collection. The two failures immediately detected were during equipment starts and catastrophic in nature with pressurized water leaking. Even these failures had early indications that were not detectable in hourly readings.

Although it does not seem like much, 2 minutes of watch per RO unit operating hour adds up to an average of 72 hours per year. Removing unnecessary man-hours from the ship's routine operation has been a major initiative over the last several budget cycles. It can be concluded that initial efforts have eliminated the obviously man-hour wastes. Remaining are incremental steps found in optimizing the smaller aspects of shipboard operation. By reducing the need and time for routine evolutions, such as logging hourly readings, the watchstander's hours are available for other necessary tasks. The summation of multiple man-hour saving increments ultimately results in the reduction of shipboard personnel.

NILM has shown, in Chapters 3 and 5, the ability to replace nine of the RO unit's output gauges and sensors on a real-time basis. These sensors include discharge pressure gauges and operating hour tachometers. Eliminating the need to log these sensor outputs cuts the time to record the readings in half. Another benefit is a reduction in sensor calibration time. Since these gauges would no longer be logged, the 15 minutes per year needed to calibrate each one is removed from the ship's maintenance man-hours.

Measures that can reduce ship man-hour demands, if they can be reliably integrated into the total ship system, are very attractive given today's budget tightening initiatives. The key, however, is taking existing man-hours off the ship without adding additional training or support equipment requirements. NILM, in its current form, has been operational onboard two U.S. Coast Guard Cutters for more than four years. During this time the computers and data collection boards have had no failures, in fact support needs have only included occasional software upgrades. This is very remarkable considering these components are "off-the-shelf" and not *hardened* against the high humidity, corrosive, and motion-intensive shipboard environment. Future versions of NILM machines promise to be even more reliable as subassemblies mature and become smaller.

6.2.2 Maintenance Costs

NILM provides a ship's crew with three major maintenance tools: condition-based maintenance, trend analysis, and immediate failure detection. Although these tools are already employed in current shipboard maintenance practices, they are not utilized on a full-time basis. NILM is capable of monitoring and providing real-time analysis that can be used by ship's force to initiate immediate and future maintenance actions. The use of NILM could, in practice, eliminate unnecessary preventative maintenance and reduce the occurrence of major equipment failures.

First, it measures electrical signals for unusual profiles and frequencies. This enables condition-based maintenance (CBM) on many system components. For example, vibration analysis tests are conducted on motors to measure bearing and shaft conditions. The results of these tests can lead to motor overhaul or replacements. Unfortunately, a vibration analysis team, special equipment, and pier-side access are required to perform the test, which counters timely problem detection. For a critical crew support system, like the RO unit, an untimely underway motor failure would severely affect the entire ship's mission capabilities. As shown in Section 0, NILM is capable of detecting CBM indicators in real-time for failing motors and pumps by assessing electrical signal demands. With a software modification, NILM could provide early detection of imminent component failures allowing the crew lead-time to optimize equipment repairs and order critical materials.

Second, by continuously monitoring a system's electrical power demand, NILM has inherent trend analysis capabilities. As shown in Chapter 5 and reference [6], mechanical systems often have key parameter trends that precede a failure. Tracking and reporting these trends is an ideal use for current NILM configuration.

Finally, immediate failure detection followed by controlling actions is a common method used to mitigate equipment damage. Unfortunately, as shipboard systems becoming more complicated and autonomous, their failures are less obvious and harder to detect, often increasing the scope and cost of the repairs. These circumstances occurred twice, as discussed previously in Section 3.3, on the RO units within the last year. An internal membrane seal failure prevented the RO unit from making freshwater for two days while the crew tried to reset the system. This failure was captured immediately by NILM with a noticeable power demand drop to the HP pump. Access to this information would have prompted the crew to secure the RO unit, preventing contamination of the potable water storage tanks and reducing the overall time to effect repairs. The other incident was the $28,000 HP positive displacement pump replacement caused by debris ingestion into the piston cylinders. Over the course of the several weeks, the ceramic pistons destroyed the pump cylinders walls as they deteriorated leading to a catastrophic failure of the entire assembly. Again, NILM caught the early stages of the failure and, if properly configured, could have alerted the crew of the problem. An immediate repair upon first detection would have only cost $300 for a new set of ceramic pistons. Mitigating the magnitude of equipment failure is a major precept of engineering casualty control procedures used by the U.S. Navy and Coast Guard. A properly integrated NILM could shorten response times for initiating these procedures, ultimately reducing the magnitude and cost of equipment failures.

As shipboard engineering plants become more dependent on remote sensors to monitor system operation [1] the maintenance demand and reliability of the sensor networks becomes a burden. A convenient facet of NILM is that it only requires two additional sensors to provide the crew with a detailed array monitoring and diagnostics tools. Additionally, these sensors, a current transducer and voltage tap, are solid-state devices with better reliability and configurability than other, more complex, types of monitors.

6.2.3 Operating Costs

During normal underway conditions, the RO unit produces enough potable water for a 24-hour period in 12 hours of operation. Reducing the number of hours required to run the RO unit would cut energy and the annual maintenance costs. Improving the RO unit operating efficiency through condition-based maintenance is one approach. Another method is to "tune" the RO unit using real-time operating parameters, such as salinity and temperature, to increase product production rates and reduce component wear. At this point, NILM's ability to monitor these types of performance parameters and optimize the production rate has not been explored. Further study is needed for potential operating costs savings associated with this type of NILM application.

6.3 Cost-Benefit Analysis

The best way to measure the benefit of new system is to consider the potential cost savings. As this is a method of predicting future circumstances, several assumptions are needed for a thorough analysis. For this analysis, the RO unit operational cost was compared for two scenarios: cost of operating the equipment *with* and *without* the NILM. Since current NILM applications would not change actual potable production rate, it is assumed that the power demand for both scenarios is the same throughout the life of the RO unit. This means that costs of energy to run the RO unit is not included in the analysis. The analysis focuses on the cost of installing and maintaining the NILM as compared to savings outlined in the previous sections. The following assumptions, not already discussed, are based on events encountered during the last two years of NILM field data collection.

General assumptions for both scenarios:

- A USCG Cutter is underway for 180 days per year
- 30 years is the minimum "lifetime" of a Cutter
- The RO unit is used only underway
- The RO unit is online for 12 hours each day underway
- The average cost of a sailor in the U.S. Coast Guard is $103,700 per year
- The average sailor stands 8 hours of watch per day underway
- The average sailor does 6 hours of equipment maintenance and repair work per day underway
- The average cost of a sailor per hour of work or watch underway is $20.29/hour

- 3% is the average inflation rate for the next 30 years

RO unit costs *without* NILM assumptions:

- A major failure has a mean time to failure (MTTF) of 8,640 hours with a material cost of $20,000 and 28 man-hours to repair
- A minor failure has a MTTF of 4,320 hours with a material cost of $8,000 and 12 man-hours to repair
- The watch takes an average of 2 hours to diagnose and initiate controlling actions for a failure
- The watchstanders requires 2 minutes of each hour while the RO unit is operating to log the gauge and sensor readings

RO unit costs *with* NILM assumptions:

- NILM does not change the RO unit potable water production rate
- A major failure has a MTTF of 8,640 hours with a material cost of $10,000 and 16 man-hours to repair
- A minor failure has a MTTF of 4,320 hours with a material cost of $2,000 and 10 man-hours to repair
- The watch takes an average of 5 minutes to diagnose and initiate controlling actions for a failure using NILM
- The watchstanders requires 1 minute of each hour while the RO unit is operating to log the minimum gauge and sensor readings
- The commercial version of the RO unit NILM software will be a one-time cost of $10,000 to develop and test
- The initial RO unit NILM installation will cost $800 and 12 man-hours per ship[7]
- RO unit NILM maintenance will cost $100 and 1 man-hour per year
- A NILM failure has a MTTF of 12,960 hours with a material cost of $500 and 2 man-hours to repair

Applying the above assumptions, the maintenance and repair costs models *with* and *without* the NILM were analyzed. Figure 6-2 represents the predicted cash flow diagrams for the two scenarios and a third scenario without the $10,000 RO unit NILM development and testing cost. Cost savings for the installation of NILM on additional ships based on economy of scale for repair and maintenance were not included. These savings are dependent on supplier availability and number of units required, making them very hard to predict. Looking at the diagram it becomes very clear that mitigating failure magnitude is crucial to cost savings.

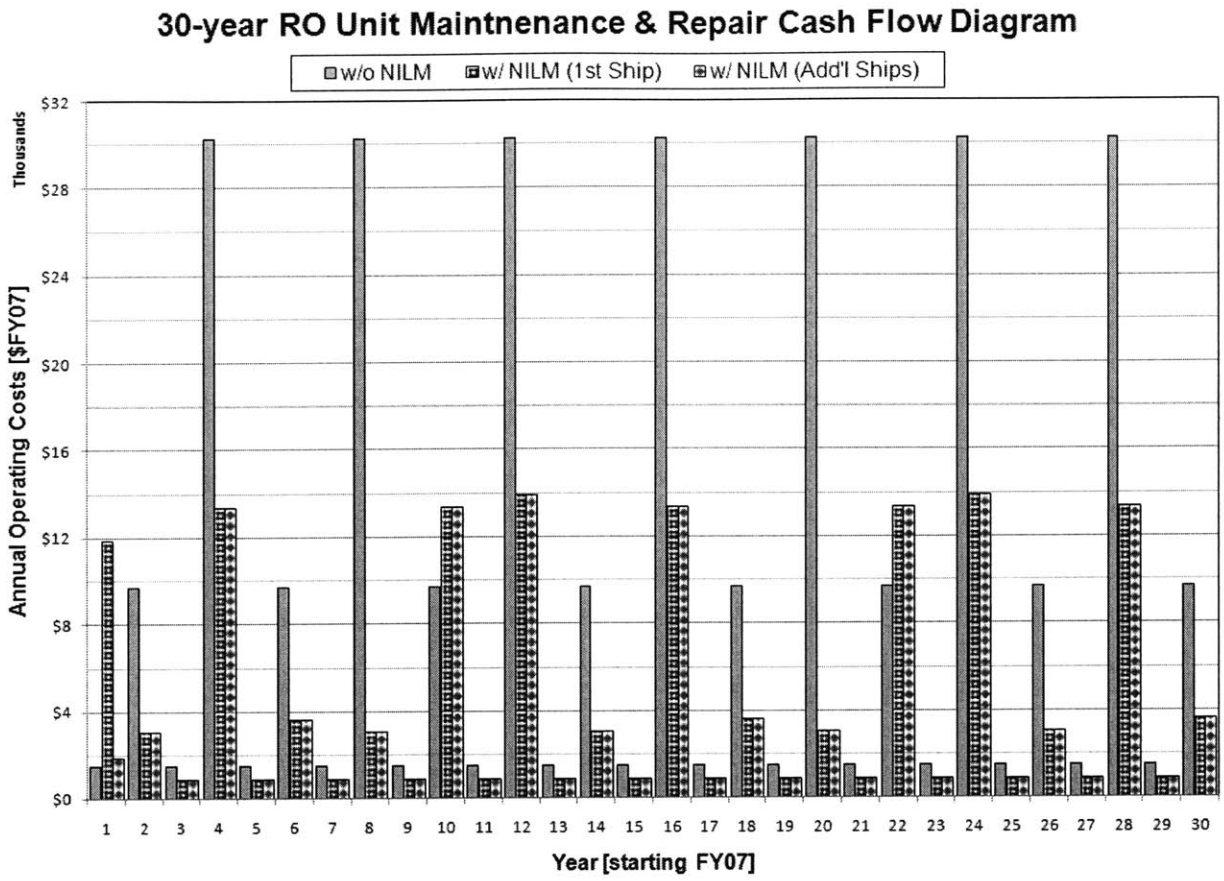

Figure 6-2: Predicted RO Unit Maintenance and Repair Cash Flow Diagram

Costs associated with mission degradation due to vital equipment failure were purposely not examined. These costs include ripple effects on fleet-wide operations, as other ships need to augment their schedules to fill mission gaps. Unfortunately, these costs are not understood until after the event occurs and, even then, hard to quantify. Table 6-1 provides the net present values of the three scenarios illustrated in Figure 6-2.

Table 6-1: RO Unit NILM Scenarios Net Present Values

Scenario	Net Present Value [$FY07]
RO Unit *without* NILM	$522,515
RO Unit *with* NILM (1st ship)	$237,465
RO Unit *with* NILM (Add'l Ships)	$227,156

Although the savings realized by using NILM may seem small compared to the ship's billion-dollar total life cycle cost, they only reflect the benefits to the RO unit. The cost savings could

quickly multiply if NILM is simultaneously installed on other vital shipboard systems and able to provide similar maintenance tools. Additionally, if the savings are applied to an entire ship class they can easily become millions of dollars per year.

6.4 Conclusions

The cost of allowing the continued operation of failing equipment becomes very prohibitive over the life of a ship. The NILM's real-time monitoring and power demand diagnostic capabilities provide the operator significant advantages with equipment failure prevention and detection. These advantages ultimately translate to major cost savings over the lifetime of the RO unit and can enhance ship dispatch reliability. Although NILM technology is primarily used on an experimental basis, its proven field deployment has shown that commercial versions are only a matter of demand.

7 Future Work and Conclusions

7.1 Proposed Future Work

During the course of data collection and analysis, several areas presented themselves with possible NILM applications. The following sections provide an outline of proposed future work with respect to the RO unit.

7.1.1 Master Control Consol Monitoring

With the multitude of controller problems reported by the crew, monitoring the master control consol (MCC) could certainly help isolate these problems and further develop the NILM as a monitoring device for the RO unit. The current NILM installation only monitors the 450-volt power to the three pump motors, since the MCC operates on 120-volt power a NILM channel would have to be dedicated to record this data. By monitoring the MCC, the NILM should be able to diagnose solenoid valve and sensor faults, ultimately aiding system diagnostics and troubleshooting.

7.1.2 RO Unit Reactive Power Analysis

The data analysis conducted to this point has strictly focused on the *real* power component of the pump motor demand. The reactive power was never evaluated for what type of information it could provide the equipment user. Given the number of transients the RO unit encounters during normal operations an examination of the reactive power may reveal another set of diagnostic indicators.

7.1.3 HP Pump Start Overshoot Transient Analysis

As shown in Figure 3-2 the HP pump power demand has an overshoot transient similar to that found in an under-damped system. Although this was observed and briefly mentioned, further analysis was not conducted on the HP pump start transient and what types of diagnostic indicators could be derived from its characteristics. By profiling the magnitude or spectral content of the overshoot signature, perhaps, the HP pump plunger wear could be determined.

7.1.4 NILM Real-Time Diagnostic Algorithm

NILM becomes most powerful when the equipment operators have immediate access to the collected data and diagnostic tools. For this type of information to be readily available to the watchstander a suite of algorithms must be developed that can analyze and diagnose equipment power demands in real-time. Several equipment condition diagnostic indicators have been discussed in this and other theses that would revolutionize current maintenance practices.

In conjunction with the diagnostic algorithm development an intuitive user interface that allows the watchstander to access and interpret data with very little training is needed for the NILM to be excepted as a true shipboard maintenance and monitoring tool. The challenge for the user interface is to balance something that is easy to use, but capable of handling the wide range of diagnostics derived from the NILM data.

7.2 Conclusion

The NILM has proven successful in capturing power demand transients and signatures with enough detail to provide a wide array of diagnostic tools. These tools range from spectral content analysis to real power demand changes. The previous chapters have demonstrated its ability to monitor, identify, and diagnose conditions on a complex and highly integrated fluid system. With its constant real-time monitoring capabilities the NILM is an ideal platform for fault detection, condition based maintenance, and trending equipment performance without the added cost and maintenance of extensive sensor networks. By monitoring the shipboard power demand, the NILM is able to provide insight on the status of many systems, both fluid and mechanical, throughout the ship without the cost and reliability issues associated with a complex sensor network.

List of References

[1]. Emma Maersk: World's Largest Container Ship. *Marine Log.* December 2006, p. 17.

[2]. **Leeb, S.B.** *A Conjoint Pattern Recognition Approach to Non-Intrusive Load Monitoring.* Cambridge : Department of Electrical Engineering and Computer Science, Massachusetts Institute of Technology, 1993. PhD Dissertation.

[3]. *Non-Intrusive Load Monitoring and Identification in an Automotive Environment.* **Shaw, S.R., et al.** Lisbon : s.n., 1999. Proceedings of ELECTRIMACS 1999. pp. 199-204.

[4]. **Shaw, S.R. and Laughman, C.R.** A Kalman-Filter Spectral Envelope Preprocessor. *IEEE Transactions: Instrumentation and Measurment.* February 26, 2004.

[5]. **Ramsey, J.S.** *Shipboard Applications of Non-Intrusive Load Monitoring.* Cambridge : Massachusetts Institute of Technology, 2004. NSEE/SM EECS Thesis.

[6]. **DeNucci, T.W.** *Diagnostic Indicators for Shipboard Systems using Non-Intrusive Load Monitoring.* Cambridge : Massachusetts Institute of Technology, 2005. SM NAME/SM ME Thesis.

[7]. **Mosman, J.P.** *Evaluation of Non-Intrusive Monitoring for Shipboard Cycling System Diagnostics.* Cambridge : Massachusetts Institute of Technology, 2006. NSEE/SM OSM Thesis.

[8]. **Shaw, S.R.** *System identification Techniques and Modeling for Non-Intrusive load Diagnostics.* Department of Electrical Engineering and Computer Science. Cambridge : Massachusetts institute of Technology, 2000. PhD Dissertation.

[9]. **Greene, W.C.** *Evaluation of Non-Intrusive Monitoring for Condition Based Maintenance Applications on US Navy Propulsion Plants.* Cambridge : Massachusetts Institute of Technology, 2005. SM NAME/SM ME Thesis.

[10]. **Shaw, S.R. and Leeb, S.B.** identification of Induction Motor parametrs from Transient Stator Current Measurements. *IEEE Transactions on Industrial Electronics.* February 1999, Vol. 46, 1, pp. 139-149.

[11]. *Development of Condition Monitoring Techniques for a Transverse Flux Motor.* **Payne, B.S., Husband, S.M. and Ball, A.D.** 2002. International Conference on power Electronics, Machines and Drives. pp. 139-144.

[12]. **Bureau of Naval Personnel.** *Principles of Naval Engineering.* Washington DC : U.S. Government Printing Office, 1987. NAVPERS 10788-B1.

[13]. **Engineers Edge.** Centrifugal Pump Flow Types. *engineersedge.com.* [Online] 2007. [Cited: April 26, 2007.] http://www.engineersedge.com/pumps/pump_menu.shtml.

[14]. **Village Marine Tec.** *Model RC7000 Plus Reverse Osmosis Desalination Plant Operations and Maintenance Manual.* Gardena, CA : Village Marine Tec, 2004.

[15]. **Zarambo, F.** Desalination Plants. [book auth.] R. ed. Harrington. *Marine Engineering.* Jesey City : Society of Naval Architects and Marine Engineers, 1992.

[16]. **SETRA Systems Inc.** *SETRA Model 230 Installation Guide.* Boxborough, MA : s.n., 2001.

[17]. **Munson, B., Young, D. and Okiishi, T.** *Fundamentals of Fluid Mechanics.* New York : John Wiley and Sons, 1998.

[18]. **Volk, M.** *Pump Characteristics and Applications.* Boca Raton : CRC Press, 2005.

[19]. **Isermann, R.** *Fault-Diagnosis Systems.* Berlin : Springer-Verlag, 2006.

[20]. *Component-Based Multi-Model Approach for Fault Detection and Diagnosis of a Centrifugal Pump.* **Wolfram, A., et al.** Arlington : s.n., 2001. Proceedings American Control Conference (ACC).

[21]. **Wood, D.J., et al.** Numerical Methods for Modeling Transient Flow in Distribution Systems. July 2005, Vol. 97, 7.

[22]. **Hogan, N.** Modeling, Analysis, and Control of Physical Systems. *Course notes for MIT course 2.151: Advanced System Dynamics and Control.* 1989.

[23]. **Kallesoe, C.S. and Izadi-Zamanabadi, R.** Model Based Fault Detection in a Centrifugal Pump Application. *IEEE Transactions Control Systems Technology.* March 2006, Vol. 14, 10, pp. 204-215.

[24]. **Krause, P., Wasynczuk, O. and and Sudhoff, S.** *Analysis of Electric Machinery.* New York : McGraw-Hill, 1986.

[25]. **Government Accounting Office.** *Navy Actions Needed to Optimize Ship Crew Size and Reduce Total Ownership Costs.* Washington DC : Government Accounting Office, 2003. GAO-03-520.

[26]. **Department of Defense.** *Department of Defense Budget for Fiscal Year 2007: Financial Summary Tables.* s.l. : Department of Defense, 2006.

[27]. **Department of the Navy.** *Department of the Navy Fiscal Year (FY) 2008/2009 Budget Estimates: Military Personnel, Navy.* Washington DC : Department of the Navy, 2007.

Appendix A RC7000 Plus Detailed Line Drawing [14]

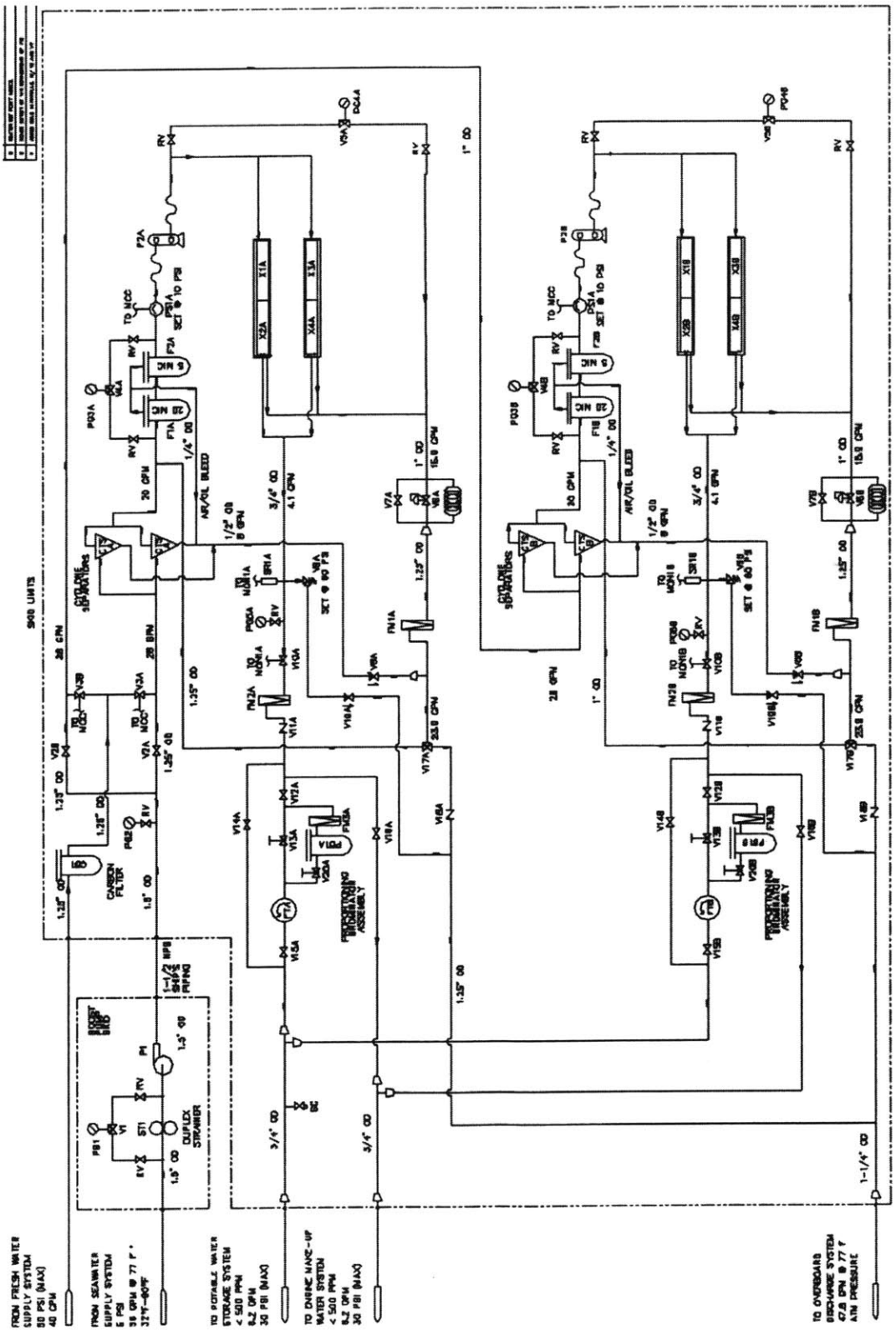

Appendix B Spectral Content Analysis MATLAB® Script

```
% fft_code.m

% r contains the data to be examined.

r=P;  %load data
st=3.5e5; %starting point of analysis


y=detrend(r(st:st+1e3));   % Remove the mean, default range of data 1e3

%plot(y);

N = 2048;  % Number of points in fft
f_sample = 120;  % NILM sampling frequency

Y = fft(y'.*hanning(length(y))',N);

f=[0:1:N/2-1]*(f_sample/N);

figure(1);
clf;
hold off;
semilogy(f,abs(Y(1:length(Y)/2)));
xlabel('Frequency: Hz');
ylabel('Magnitude');


figure(2);
clf;
hold off;
plot(f,abs(Y(1:length(Y)/2)));
xlabel('Frequency: Hz');
ylabel('Magnitude');
```

Appendix C Laboratory Test Stand MATLAB® Scripts

Data Conversion

```
% brute_conv_starts('f:\matlab71\work\Brute_data')

function brute_conv_starts(path)
%path='c:\matlab71\work\Brute\test';

strP1 = sprintf('%s/*P1.txt',path);
strQ1 = sprintf('%s/*Q1.txt',path);
strP2 = sprintf('%s/*P2.txt',path);
strQ2 = sprintf('%s/*Q2.txt',path);
strDPP = sprintf('%s/*DPP.txt',path);
strFL = sprintf('%s/*FL.txt',path);
strRM = sprintf('%s/*RM.txt',path);
strDPF = sprintf('%s/*DPF.txt',path);

filesP1 = dir(strP1);
filesQ1 = dir(strQ1);
filesP2 = dir(strP2);
filesQ2 = dir(strQ2);
filesDPP = dir(strDPP);
filesFL = dir(strFL);
filesRM = dir(strRM);
filesDPF = dir(strDPF);

info = size(filesP1);

power = struct([]);
disp('working...');
path = regexprep(path, '\', '/');

for i=1:1:info(1)
   i

   %% Run Time Setup %%
   str = sprintf('%s/%s',path,filesDPP(i).name);
   data=load(str);
   time=length(data)/8000;  %time=number of seconds

   countraw_a=length(data);
   countraw=length(data);

   % Start Time
   x=[]; j=1;  %resets x and j
   A1 = diff(data);
   while j <= length(A1)
       if A1(j)>40  %adjusts upcrossing threshold
           countraw_a = j;
           break
       end
       j=j+1;
```

```
end

% Cross Check
str = sprintf('%s/%s',path,filesDPF(i).name);
data=load(str);
x=[]; j=1;  %resets x and j
A1 = diff(data);
while j <= length(A1)
    if A1(j)>40  %adjusts upcrossing threshold
        countraw = j;
        break
    end
    j=j+1;
end

if countraw_a < countraw
    countraw = countraw_a;
end

rtime = length(data)/8000 - 1;
tstartraw = countraw/8000;

%% count prep data
str = sprintf('%s/%s',path,filesP1(i).name);
data=load(str);
time=length(data)/8000;  %time=number of seconds

countprep_a=length(data);
countprep=length(data);

% Start Time
x=[]; j=1;  %resets x and j
A1 = diff(data);
while j <= length(A1)
    if A1(j)>40  %adjusts upcrossing threshold
        countprep_a = j;
        break
    end
    j=j+1;
end

% Cross Check
str = sprintf('%s/%s',path,filesDPF(i).name);
data=load(str);
x=[]; j=1;  %resets x and j
A1 = diff(data);
while j <= length(A1)
    if A1(j)>40  %adjusts upcrossing threshold
        countprep = j;
        break
    end
    j=j+1;
end

if countprep_a < countprep
```

```
    countprep = countprep_a;
end

tstartprep = countprep/120;

%% IMPORTING DATA using countprep and coutraw
%% Power 1 %%
str = sprintf('%s/%s',path,filesP1(i).name);
str1 = sprintf('%s/%s',path,filesQ1(i).name);
data=load(str);
data1=load(str1);
data=data(1:round(rtime*120));
data1=data1(1:round(rtime*120));
power(1).name = str;

P1 = vertcat(0, 0, abs(data(countprep:length(data),1)));
Q1 = vertcat(0, 0, abs(data1(countprep:length(data1),1)));
power(1).data = P1;
power(1).Qdata = Q1;

Ptime=(length(P1)-2)/120;
c=length(P1)-2;
t=1:c;
t=(t'./c)*Ptime;
t=vertcat(0, tstartprep, t+tstartprep);
power(1).time = t;

%% Power 2 %%
str = sprintf('%s/%s',path,filesP2(i).name);
str2 = sprintf('%s/%s',path,filesQ2(i).name);
data=load(str);
data2=load(str2);
data=data(1:round(rtime*120));
data2=data2(1:round(rtime*120));
power(2).name = str;

P2 = vertcat(0, 0, abs(data(countprep:length(data),1)));
Q2 = vertcat(0, 0, abs(data2(countprep:length(data1),1)));
power(2).data = P2;
power(2).Qdata = Q2;

Ptime=(length(P2)-2)/120;
c=length(P2)-2;
t=1:c;
t=(t'./c)*Ptime;
t=vertcat(0, tstartprep, t+tstartprep);
power(2).time = t;

%% Pump Diff Pressure %%
str = sprintf('%s/%s',path,filesDPP(i).name);
data = load(str);
data=data(1:rtime*8000);
power(3).name = str;
power(3).data = data(:,1);
t=1:length(data);
```

```
t=t'./8000;
power(3).time = t;

%% Flow Meter %%
str = sprintf('%s/%s',path,filesFL(i).name);
data = load(str);
data=data;
power(4).name = str;
%
A1 = abs(diff(data));
top=[countraw]; j=1;
while j <= rtime*8000
    if A1(j)>100  %adjusts upcrossing threshold
        top = [top,j];
        j=j+10;  %adjusts spacing after upcrossing
    else
        j=j+1;
    end
end
kfactor = 29.46; %cycles/gal
gpm = (8000*60)./(kfactor.*diff(top)); %gal/min
gpm = horzcat(0, 0, gpm, 0);
power(4).data = gpm;
power(4).rawData = data./max(data);
%
t=top./8000;
t=vertcat(0, t', rtime);
power(4).time = t;

%% Pump Motor RPM %%
str = sprintf('%s/%s',path,filesRM(i).name);
data=load(str);
data=data;
power(5).name = str;
%
top=[]; j=1;  %resets top and j
A1 = (diff(data));
while j <= rtime*8000
    if A1(j)>100  %adjusts upcrossing threshold
        top = [top,j];
        j=j+10;  %adjusts spacing after upcrossing
    else
        j=j+1;
    end
end
rpm = (8000*60)./diff(top);  %rev/min
rpm = horzcat(0, 0, rpm, 0);
power(5).data = rpm;
%
t=top./8000;
t=vertcat(0, t', rtime);
power(5).time = t;

%% Filter Diff Pressure %%
str = sprintf('%s/%s',path,filesDPF(i).name);
data = load(str);
```

```
    data=data(1:rtime*8000);
    power(6).name = str;
    power(6).data = data(:,1);
    t=1:length(data);
    t=t'./8000;
    power(6).time = t;

    path = regexprep(path, '/', '\');
    str = regexprep(filesP1(i).name, 'P1.txt', '.mat');
    s = power;
    save(str,'s');
%
    delete(filesP1(i).name);
    delete(filesQ1(i).name);
    delete(filesP2(i).name);
    delete(filesQ2(i).name);
    delete(filesDPP(i).name);
    delete(filesFL(i).name);
    delete(filesRM(i).name);
    delete(filesDPF(i).name);
 %
    power = struct([]);
end
```

Data Plotting

```
% brute_plot.m                                          Version: 1.0
% By: Gregory R. Mitchell                               Updated: 13 SEP 2006

% Use to plot Brute multi-channel NILM data from '.mat' file format.

% INPUTS %
% use 'path' to set directory, example: 'c:\matlab71\work\RO_LP\PQ'
% use 'file_name' to ID starting point, example: '20060501-05'

% OUTPUTS %
% 'brute' is the file that was used for the plots

% INPUT LINE EXAMPLE %
% [brute]=brute_plot('c:\matlab71\work\brute_data','1_2_0927');

% FOR TESTING %
%path='c:\matlab71\work\RO';date_time='20060813-05';time=24;type=3;chan=4;

function [brute] = brute_plot(path,file_name)

% DATA FILE COLLECTION %
str = sprintf('%s/*.mat',path);
files = dir(str);
info = size(files);

% DATA FILE SEARCH %
for i=1:info(1)
    z = regexp(files(i).name,file_name);
```

```
    if z > 0,
        n=i;
        break
    end
end

% DATA COLLECTION %
str = sprintf('%s/%s',path,files(n).name);
brute = load(str);

P1 = brute.s(1).data;
tP1 = brute.s(1).time;
P2 = brute.s(2).data;
tP2 = brute.s(2).time;
DPP = brute.s(3).data;
tDPP = brute.s(3).time;
FL = brute.s(4).data;
tFL = brute.s(4).time;
RM = brute.s(5).data;
tRM = brute.s(5).time;
DPF = brute.s(6).data;
tDPF = brute.s(6).time;

% PLOTTING %
figure(2)
subplot(4,1,1);
plot(tP1, P1, tP2, P2)
title(sprintf('%2.0f-sec plot of Brute run: %s', max(tP1), files(n).name));
ylabel('Power');
axis tight
grid on;

subplot(4,1,2);
plot(tDPP, DPP, tDPF, DPF)
ylabel('DP Gauges');
axis tight
grid on;

subplot(4,1,3);
plot(tFL, FL)
ylabel('Flowmeter [gpm]');
axis tight
grid on;

subplot(4,1,4);
plot(tRM, RM)
ylabel('Tachometer [rpm]');
xlabel('Time [sec]');
axis tight
grid on;
```

Appendix D Thesis Data CD Contents

The Thesis Data CD is available in The Laboratory for Electromagnetic and Electronic Systems (LEES) or on the lab's data storage network (`bucket.mit.edu`).

Disk Title: Fluid System Diagnostics using NILM

Folders and Files:

Documents
- ASNE Papers – NILM related papers written over the last year
- Brute – Laboratory Test Stand component specification sheets and pictures
- CT Specs – NILM current transducer specification sheets
- Line Drawings – *Seneca* line drawings for the ASW, RO, and steering systems
- NILM Theses – Previous NILM theses
- Presentations – Thesis poster and power points of RO NILM progress
- References – Various references used to analyze and model fluid systems
- RO – RO component specification sheets, pictures, and spreadsheets used for analysis

MATLAB Files
- Data
  - Brute – Data files from clogging, cavitation, and pump curve experiments
  - CBM – Condition based maintenance files used for the RO HP pump
  - RO – Snapshot files from RO NILMs
- Figures – Figures generated from collected data used in thesis
  - Brute – Figures generated from Brute data used in thesis
- Scripts
  - Brute – m-files used to analyze Brute data
  - RO – m-files used to analyze RO data
  - CBM_fft.m – code used to conduct condition based maintenance analysis
  - fft_code.m – code used to plot real power spectral content
  - P_convert.m – code used to convert *prep* data from NILMs to kilowatts
  - prep_to_current.m –calculates the conversion factor used in P_convert.m
- Pump-Filter Model – m-files used for simulating the pump-filter start transient

Thesis
- Mitchell Thesis.docx – Word 2007 thesis document
- Mitchell Thesis.pdf – PDF of final thesis version
- Thesis Figures.pptx – Power Point 2007 figure slides